



Western Norway
University of
Applied Sciences

BACHELOR'S THESIS

Photogrammetry using UAV's

Andreas Verheyden

Thomas Jonckheere

Sil Gevaert

Bachelor in applied sciences: construction

Avdeling for ingeniør- og naturvitskap

Stig Frode Samnøy/ Trond Nordvik/ Loftur Thor

Jonsson

In cooperation with Statnett

29/05/2019

I confirm that the work is self-prepared and that references/source references to all sources used in the work are provided, cf. Regulation relating to academic studies and examinations at the Western Norway University of Applied Sciences (HVL), § 10.

1. Preface

This Bachelors thesis was written by Andreas Verheyden, Thomas Jonckheere and Sil Gevaert. Three construction engineering students on an ERASMUS exchange from Belgium. It was written at Western Norway University of Applied Sciences campus Bergen, Department of Civil Engineering, in the Spring semester 2019.

After a brief meeting with a representative of Statnett, Frode Kutschera discussing alternatives for scanning power lines and interesting sites. The research included making a 3D model of a test area using photogrammetry with the help of an UAV.

The idea to use drones with photogrammetry was very interesting for us. None of our group had any prior experience with drones and photogrammetry. During the completion of the assignment we learned how photogrammetry worked and how it can be implemented.

We would like to express our sincere gratitude to Stig Frode Samnøy and Trond Nordvik for helping us with our questions and giving feedback during this research. We would like to thank Loftur Jonsson for his help In finding a fitting study for our group.

Andreas Verheyden Thomas Jonckheere Sil Gevaert

Bergen, May 2019

2. Abstract / Sammendrag

English

In this report we are going to discuss the procedure of making a point cloud from an area using photogrammetry with the help of an UAV. The different problems and their solutions are discussed in this report as well. We compared the results of 2 different drones and a dataset from a Norwegian website with datasets, namely Høydedata. Lastly a comparison was made with group B23, to see the differences between the drone and terrestrial laserscanning.

The purposes of drones in construction and surveying increase by the day. They are an asset in many construction and surveying applications. The utilized drones are both models of DJI. The models are the Mavic PRO and the Phantom4RTK. The Phantom4RTK uses a D-RTK 2 base station with RTK technology.

We concluded that drones are a good alternative to methods currently employed by Statnett, albeit with some limitations. It is the fastest and easiest method to acquire data, with a sub 0.2m overall accuracy. The technique is limited by certain parameters, namely the requirement of a line of sight to the drone, accessibility of an area and the batteries. The laserscanning was a better option for data acquisition of the electricity pylons themselves, while the drone is more suited for terrain modelling.

Norwegian

I denne oppgava diskuterer vi framgangsmåten for å lage en 3d-modell av et areal ved å bruke fotogrammetri med hjelp av en UAV. De ulike problemene og løsningene ved prosessen blir også drøftet. Vi sammenlignet resultatene fra 2 ulike droner og fra Høydedata, som er et sett med data fra ei norsk nettside. Til slutt sammenlignet vi resultatene også med B23 gruppa for å se på ulikhetene mellom skanninga med dronen og laserskanninga på bakken.

Droner blir stadig viktigere for bygging og kartlegging. De er et viktig hjelpemiddel i mange byggings- og kartleggingsprogrammer. Begge droner som vi brukte er DJI-modeller, resp. Mavic PRO og Phantom4RTK. Phantom4RTK bruker D-RTK 2 landingsenhet med RTK teknologi.

Vi konkluderte med at droner er et godt alternativ til metodene som blir brukte av Statnett nå for tida, selv om de har en del begrensinger. Det er den raskeste og letteste metoden for å samle inn data, med en nøyaktighet av sub 0.2m. Prosedyren er likevel begrenset av visse faktorer, altså behovet for siktelinje, tilgjengelighet av området og batterier. Laserskanninga virket bedre for datainnsamlinga enn selve kraftpylonene, mens dronen er mer egnet til terrengmodellering.

3. Table of contents

1. Preface	1
2. Abstract / Sammendrag	2
3. Table of contents	3
4. List of abbreviations	5
5. Introduction	6
6 Background	6
6.1 Statnett	6
6.2 Power grid	6
6.3 Towers	7
6.4 Test Area	7
6.5 Drones	8
6.6 Helicopter scanning	8
7 Problem description	8
8 Drones	9
8.1 Laws and regulations	9
8.2 Weather	9
8.3 Dji Mavic Pro	10
8.4 Dji Phantom 4 RTK	10
9 Method	11
9.1 Before going out	11
9.2 On site	12
9.2.1 First and second scan	12
9.2.2 Third scan	13
9.3 After the scan	13
10 Software	13
10.1 Pix4D	14
10.1.1 Functionality	14
10.1.2 User-friendliness	16
10.2 Agisoft Metashape Professional	17
10.2.1 Functionality	17
10.2.2 User-friendliness	18
10.3 ARCGis Drone2Map	18
10.3.1 Functionality	18
10.3.2 User-friendliness	19
11 Theory	20

11.1	Navigation system.....	20
11.1.1	GNSS.....	20
11.1.2	GPS.....	20
11.1.3	RTK.....	21
11.2	Photogrammetry.....	22
11.2.1	Introduction.....	22
11.2.2	How does it work?.....	22
11.2.3	When do we use photogrammetry?.....	22
11.2.4	How do we use it in geoscience?.....	22
11.2.5	The important aspects.....	23
12	Results.....	37
12.1	General results.....	37
12.2	Discussion of the results.....	46
12.2.1	Overlap.....	46
12.2.2	Error contribution.....	46
12.2.3	Total inaccuracy and uncertainty.....	46
12.2.4	Processing time and load.....	46
12.3	Influence of snow on results.....	47
12.4	Comparison with Høydedata.....	47
12.5	Flight plan accuracy.....	48
12.6	Comparison with terrestrial laserscanning.....	48
	Practical experiences.....	48
	Comparison devices.....	48
12.7	Conclusion of the report.....	49
13	References.....	50
14	List of figures.....	52
15	List of tables.....	54

4. List of abbreviations.

LiDAR: Light Intensity Distance and Ranging

RTK: Real Time Kinematics

GNSS: Global Navigation Satellite System

DGNSS: Differential Global Navigation Satellite System

GPS: Global Positioning System

UAV: Unmanned Aerial Vehicle

GloNaSS: Global Navigation Satellite System

GSD: Ground Sampling Distance

GCP: Ground Control Point

LOD: Level Of Detail

5. Introduction

The goal of this research is to analyse and compare 3D measurements from dronescanning to methods that are currently in use by Statnett. There are two main areas of interest: the exploration of a method for data acquisition for terrain models and making a comparison of the acquired data with existing terrain data. The data will also be compared to data from terrestrial laserscanning from group B23.

6 Background

6.1 Statnett

Statnett is a state enterprise whom is responsible for the system operating of the Norwegian power grid. It maintains and builds the power lines that ensure the entirety of Norway is provided with energy. Another facet of the enterprise is maintaining a balance between the production and consumption of electrical power. The main power source in Norway is hydroelectrical power.

Statnett owns the majority of the transmission grid. Only 6% (Norwegian Ministry of Petroleum and Energy, 2015) of the regional grid isn't owned by Statnett; the company rents these from the other grid companies.

6.2 Power grid

The power grid in Norway is split in 3 sections. First there is the transmission grid, which connects consumers and producers in a national system. There are connections with other countries, such as the Nordic countries and the Netherlands among others. Said grid uses a high operating voltage: it is usually between 300 and 420 kV. Statnett is the system operator of this power grid.

Another level of the power grid is the regional grid. This grid may include production and consumption, and mostly functions as the connection between the transmission grid and the distribution grid. It uses a fairly high voltage, between 33 and 132 kV. Lastly, there is the distribution grid. These are all the local grids that transport the power to the smaller end users. It is split up in high- and low voltage parts. The max voltage transported through this grid is 22 kV. The high voltage segments output is approximately 1 kV, while the low voltage segments carry 400 or 230V for the end user.

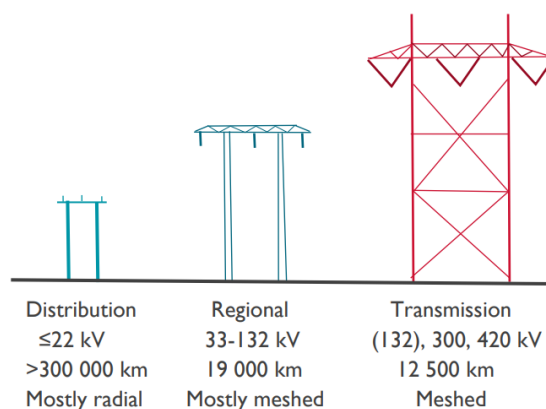


Figure 1 Types of towers (Norwegian Ministry of Petroleum and Energy, 2015)

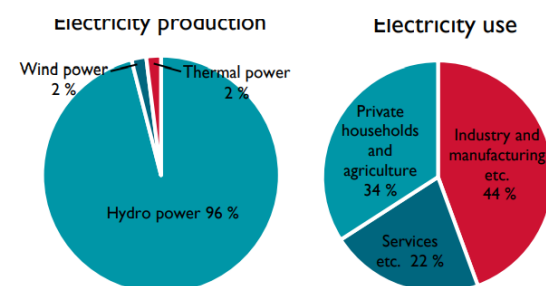


Figure 2 Energy production and consumption in Norway (Norwegian Ministry of Petroleum and Energy, 2015)

The production of electricity finds its way into the grid through both the regional and transmission grids. High end consumers are connected to these grids instead of the distribution grid. Lower power consumption applications, such as households and small scale manufacturing, are connected through the distribution grid.

The electricity production capacities of Norway come almost exclusively from hydropower at this moment. Only a small fraction comes from wind or thermal power. Private households and agriculture use approximately 34% of the generated power, services 22% and the rest 44%.

6.3 Towers

Every tower in the vicinity of the test site is of the meshed type. These are part of the transmission grid. This means that the towers operate on 300 to 420 kV. This may cause problems for the drones; the electromagnetic field is the strongest of all the towers. Experience taught us that the closer the drone got to the tower, the more difficult it became to keep the drone stable. This can be explained by electromagnetic interference from the the powerlines themselves.



Figure 3 Electricity pylon at test site (own image)

6.4 Test Area

Our test site is located at the very end of Totlandsvegen in Nesttun. The site in question consists of 2 towers, with a distance of approximately 300m between each other. The towers

are located on top of a plateau, close to the flanks of the plateau. The plateau was covered in a layer of snow during the initial measurements. At the time of the second flight, all of the snow had melted. This gave us the opportunity to see if snow has a direct influence on the results. There were no trees or other large vegetation in the area. Both towers were constructed 440m above sea level.



Figure 4 Test area (Høydedata, 2016)

6.5 Drones

In our case we used 2 drones to scan the area on separate occasions. The Mavic Pro is a drone intended for photography and filmography, while the Mavic Phantom 4 RTK is made to be used for mapping purposes. This implies that the Phantom 4 RTK should yield more accurate and thus more usable results for our purposes.

6.6 Helicopter scanning

Scanning by the use of an aerial LiDAR system in a helicopter is the current method of data acquisition for Statnett. One of the main disadvantages of this solution is that the planning and execution of the flights take a long time (1 year or more). The data provided is limited as well. Depending on the flying height, the density of the point cloud fluctuates heavily.

7 Problem description

The main objective of this report and research is analysing if drones can replace certain current techniques for the acquisition of data for Statnett. The main focus of the research is how we can produce the best, most accurate terrain model through the use of a drone. A secondary objective may be the use of drones to acquire data to construct a model of the powerlines themselves and classify the parts of these towers.

8 Drones

Nowadays drones get more and more useful in different branches all over the world. In this work we have explored the use of drones in geographic mapping. We also had a look at the difference between mapping with drones versus with a helicopter.

For the drone mapping we used 2 different drones with each of them a different camera and navigation accuracy. This is useful to determine the influence and how applicable the different systems are.

The use of drones in the field requires certain steps before the flight can be initiated. Next to weather, the legal aspect is important for the deployment of drones. The UAV returns to the base station if the battery dips under 30%. This is programmed in this way to ensure a safe landing.

8.1 Laws and regulations

You don't need a permit when you use your drone for non-commercial purposes. But because we undertook this project for Statnett we followed the rules for commercial purposes. This means that we were required to have a permit and insurance.

There are a lot of rules and regulations about drones and how to use them. But the following rules are the most important ones that were applicable to us.

When flying a drone, this should be done in such manner that there is no risk of harming people, animals or even properties and other aircrafts. To help accomplish this the drone must be clearly visible to the drone pilot at all times. If there were to be a loss of control, all drones should be equipped with a fail-safe system that will land the drone automatically. This system should also engage in case the main radio communication system fails. Nobody is allowed to fly a drone when under the influence of alcohol or drugs.

While flying the drone, the pilot in command and the pilot should use an altimeter or another method to determine the height of the drone. This is needed to make sure that the drone doesn't fly higher than the prohibited 120 metres above ground or water.

You cannot fly a drone above prisons, military bases or government buildings except with permission from the local person in charge. Drones are not allowed to fly in a no-fly zone or closer than 5km to an airport (except with permission from the person in charge of the airport). It is also not allowed to fly over a site of an incident where armed forces or emergencies services are involved.

8.2 Weather

The main issues that can arise are consequences of wind and or humidity. To ensure good results, wind, rain, mist, snowfall,...etc should be a deciding factor on the use of the drone. Any indication of problematic weather conditions means a no go to undertake a flight.

In case of any kind of fall (rain, snow, hail, etc.) the flight is to be cancelled immediately. These conditions endanger the drone, and ensure that the measurements extracted from the photos will be inaccurate. It is therefore better to plan the flight on another occasion.

Minor wind (less than 36km/h) is acceptable for the flight of drones. More wind decreases accuracy of the measurements and makes the flight more difficult. No wind at all would be the ideal situation.

Cold weather has a major influence on battery life as well. In our experience, colder weather means shorter battery life. For prolonged flights in cold weather it is advised to bring multiple spare battery packs.

8.3 Dji Mavic Pro

The drone that was used for the first flight was a Dji Mavic Pro (Figure 5) made by the Chinese company Dji. The drone in this instance was owned and operated by a drone pilot from Statnett. Depending on the mission, the drone can fly manually or on autopilot.

This drone can fly up to 21 minutes with a 3830mAh battery. If a longer scanning time is required. You can easily switch out the batteries.



Figure 5 Dji Mavic Pro (DJI, 2019)

A mobile app on your phone will directly receive the images in real time from the drones 12MP camera. The phone can be placed in a cradle directly attached to the controller. Although the pilot can look 'through' the camera he is legally obligated to keep visual contact with the drone at all times. This is the main reason the drone has a bright orange colour. (DJI, 2019)

8.4 Dji Phantom 4 RTK

The second drone we used for the second photogrammetry flight was a Dji Phantom 4 RTK (Figure 6) by the same company as the Dji Mavic Pro (Figure 5). It is a recent device which was available and provided by HVL. Just as the previous drone the Phantom 4 can be flown manually and automatically.

This drone has a flight time of approximately 30 minutes with a 5870 mAh battery. Switching the battery is an easy process for this drone as well. (DJI, 2019)



Figure 6 Dji Phantom 4 RTK (DJI, 2019)

This drone can be used with a D-RTK 2 base station (Figure 7). This will ensure more accurate measurements. With this base station, a 0.01m level accuracy can be achieved. This system can use all of the common position signals; GLONASS, GPS, GALILEO and Beidou. Information is fed directly to the drone in real-time. It is possible to line up to 5 drones at the same time with this system. (DJI, 2019)

There are some parameters that have to be taken into consideration while using this device. It has to be level and has to be connected to the drone. It must be able to receive a signal from one of the positioning systems to function properly.



Figure 7 Dji D-RTK 2 base station (own image)

9 Method

Scanning an area is more than just flying the drone. There is a lot to be done before actually scanning and afterwards. In this segment we shall describe how and what we did to scan the test area.

9.1 Before going out

Before we went out to scan there were several things we had to check. To determine if our area was safe to fly, we had to check if it was a no-fly zone and if it interfered with any flight routes of some kind. We also had to check the weather forecast in that area, because as already mentioned this can interfere with the working of the drone. Aside from the weather we needed to make sure that the drone was ready to fly and that all batteries were fully charged, including the battery from the phone. We made sure that all our firmware and software were up to date and the settings were correct. Finally we checked if there was enough memory on the SD card to save our scan.

If all of the previous mentioned things were in order, we downloaded the map, of the area we wanted to scan, in to the Dji Go app.

9.2 On site

9.2.1 First and second scan

Even though we checked the weather beforehand, we determined on site if the weather was good enough to fly (precipitation, visibility, temperature). Then we checked if there were any potential hazards in the area (trees, people, animals, ext.). When we checked the safety, we started making a base station. This was just a flat spot where we set up our UAV for taking off and landing (when we used the Phantom 4 RTK we used a D-RTK 2 base station). The base station was used as a home spot so if something would have gone wrong we could just pressed the “come home”-button and the drone would returned to this base point. Normally, this is the point where we had to place the GCP’s but we decided not to use those to see what influence this would have on the accuracy of the scans.

We placed the drone in position, switched the controller on. When the controller was on it was time to put the battery in to the UAV. To turn on the UAV we pressed the on-button two times until the lights started flashing and it indicated that the drones was connected to the controller. Everyone got in position and the drone pilot (recognisable by his fluorescent jacket) started doing the system checks. This was just hovering and making a few turns to be sure that everything works as it is supposed to. Everything worked fine and we started the automated flight plan we determined on the app. While the drone was flying the pilot kept visual the whole time. During the flight we were checking the surroundings for any potential hazards.



Figure 9 Mavic on base station (own image)



Figure 8 Mavic during system test (own image)

9.2.2 Third scan

For this instance we did exactly the same things as the previous 2 scans. Additionally we placed GCP's. We did this to see the effect of GCP's on the accuracy. For the GCP's we used big black garbage bags (secured in to place with stones) with a steel plate in the centre. With fluorescent spray paint we marked the centre point of these plates with a checkboard pattern (Figure 10). Afterwards we measured the coordinates of the centre points with a GNSS.



Figure 10 GCP target (own image)



Figure 11 Coordinates GCP (own image)

In (Figure 12) you can see how the GCP looks from the images taken by the drone. As you see the checkerboard pattern is not clearly visible. So we recommend using a larger target where the centre is more visible.

9.3 After the scan

When the drone completed its flight plan it returned to the home/base point. After the drone was shut down we turned off the controller and started packing our stuff and filling in the logbook. Back at HVL we transferred the data. The last step was processing the data.

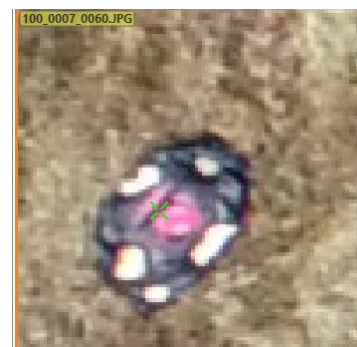


Figure 12 GCP from drone image (own image)

10 Software

Multiple software solutions were tested, to find whichever one fits the needs of this project best. The tested programs are Autodesk Recap Pro, Pix4D, Agisoft Metashape Professional and ARCGis Drone2Map. After brief initial testing, the use of Autodesk Recap Pro got scrapped because of the very limited functionality and options provided. The results generated by Autodesk Recap Pro were not suitable for use in accurate models.

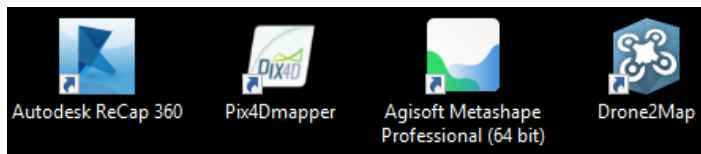


Figure 13 Software solutions (own image)

The main purpose of these programs is to acquire a usable and suitable point cloud through the use of photogrammetry. Extra functionality, such as easy access to data about accuracy aren't necessary, but increase the effectiveness of the software. Next to this, other parameters such as processing time and interface/User-friendliness aspects are valued as well.

All datasets got run through all software, with the exception of Autodesk Recap Pro. Every process was done in the same circumstances to ensure the comparison is as accurate as possible. This was done on a laptop with 8 GB of RAM and an Intel Core I7-7500U 2.70 GHz processor. Every non-vital function of the laptop was shut off.

Hardware	CPU: Intel(R) Core(TM) i7-7500U CPU @ 2.70GHz RAM: 8GB GPU: Intel(R) HD Graphics 620 (Driver: 21.20.16.4534), LuminonCore IDDCX Adapter (Driver: 1.0.2017.1023)
Operating System	Windows 10 Home, 64-bit

Figure 14 Computer specifications (own image)

10.1 Pix4D

10.1.1 Functionality

Pix4D has all the needed functionality. At the start of a project, it asks for pictures to be selected. After this, the program lets you select the degree of detail and the type of model one wants to attain from the image processing. After the processing, multiple extra viewports

can be accessed, with options from a 2D map to a fully coloured 3D model. Standard output of the processing is a point cloud.

The available viewports are the following: Map View, rayCloud, Volumes, Mosaic Editor and Index Calculator.

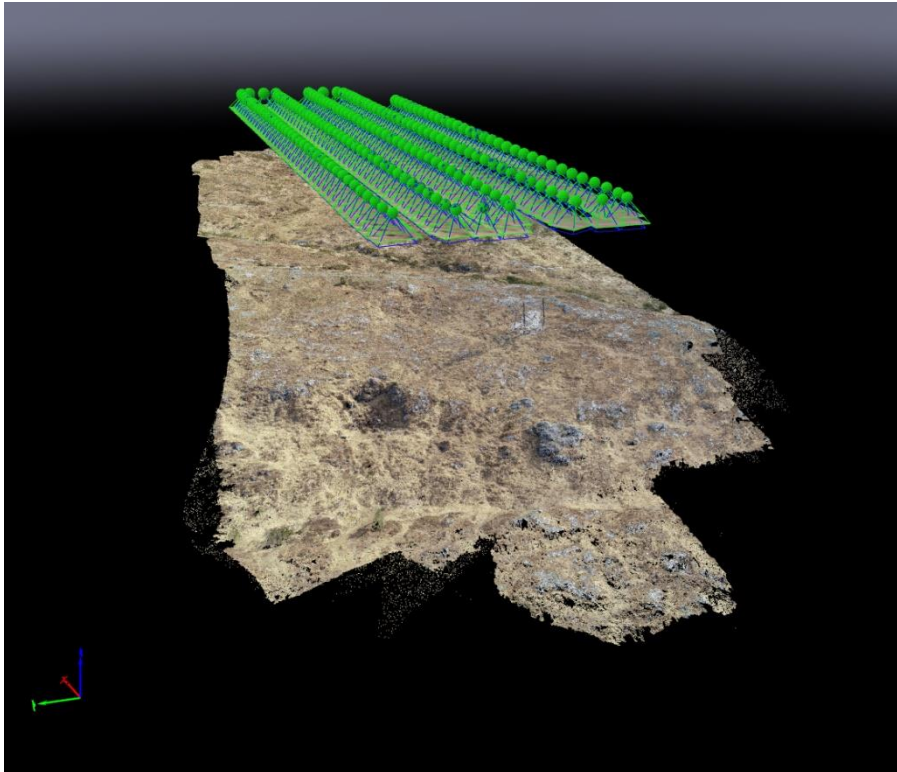


Figure 15 Pix4D point cloud (own image)

Map view shows a map overview on which the position of each taken picture is signified by a dot. The dot's colour signifies in which processing step it is at the moment. Red means it is finished.

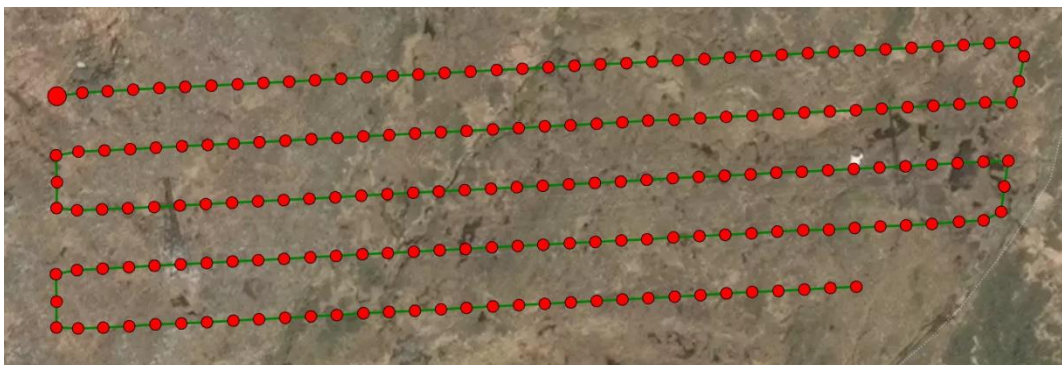


Figure 17 Flight pattern (own image)

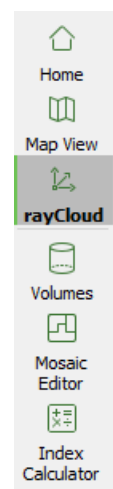


Figure 16 Pix4D options

rayCloud shows the point cloud that is generated through the software algorithm. Multiple options for filtering what is viewed on the screen are present. It gives an easy way to connect each point to the actual used images.

Volumes shows the coloured 3D model, which is the point cloud with a mesh applied, it is coloured through the pictures used for the model. This can be useful to identify any kind of water streams and or structures that are not as easily visible in solely the point cloud.

The mosaic editor allows to extract a 2D top down map of any specified region of the model. It consists of an image that is geometrically corrected. This can be used to later apply altitude. Said feature also allows easy planning of any future structures. The GNSS data embedded in the model carries over in this map.

Index calculator gives the option to generate a reflectance map and analyse the refractive index per measured point. There is a plethora of options to show this information. Regions can be selected and analysed individually.

A multitude of exportable file extensions are available, according with which viewport option you want to export. This includes, but isn't limited to .las, .tif, .xyz, .ply, .laz and others.

A quality report can be generated for the entire file, or for small selected parts of the point cloud. This file is exported in a PDF format. For the dense cloud, 13.239.370 3d points were generated in case of the first batch, and 21.158.612 for the second batch. The average point density was 596,73 and 607,74 points per cubic metre for the first and second batches of pictures respectively.

10.1.2 User-friendliness

Every function is easy to find and utilize. If you hover over the function, a popup window with a brief explanation shows up. Menu and viewports are easy to find, clear, and easy to use. Every function is well explained in the software. There are numerous tutorials and guides easily accessible.

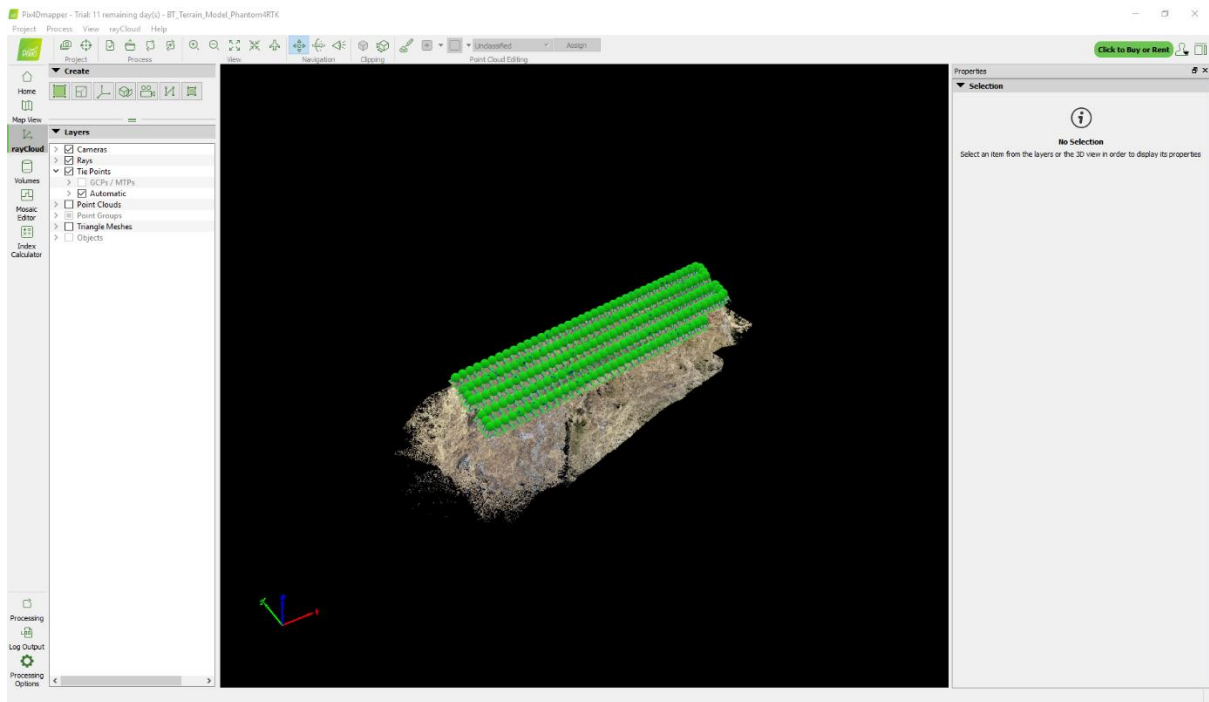


Figure 18 Pix4D user interface (own image)

10.2 Agisoft Metashape Professional

10.2.1 Functionality

The software has the basic options for the processing of the images itself. It lacks the extra viewport options Pix4D provides. Extra processing cycles can be utilized to make the point cloud more dense. This has limited effect on the results for this project.

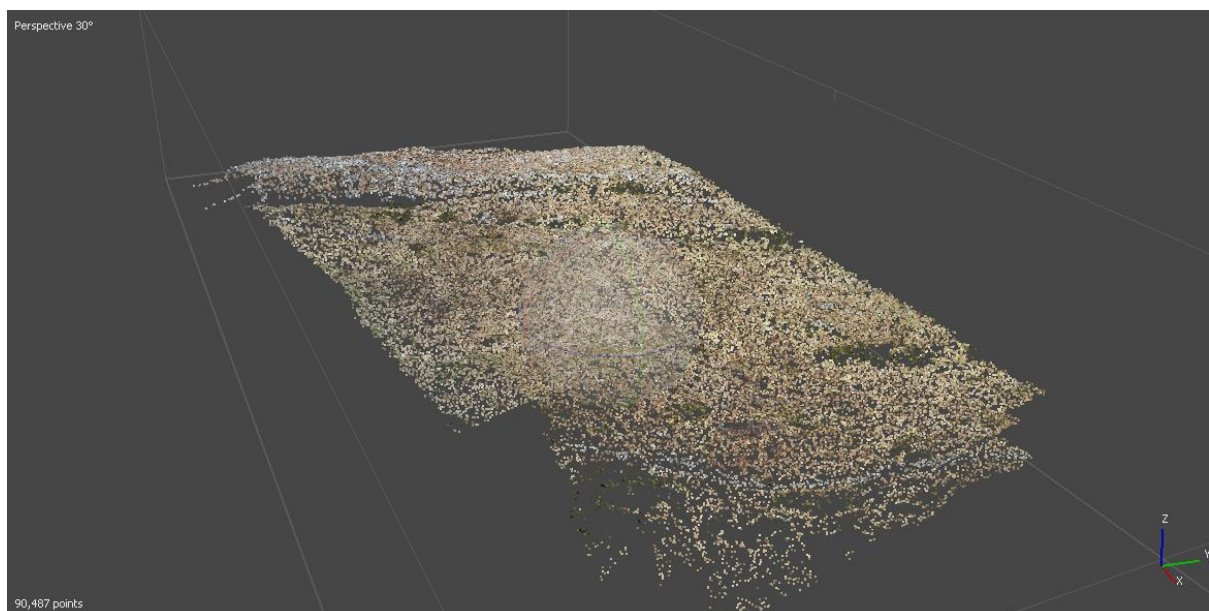


Figure 19 Agisoft Metashape Professional point cloud (own image)

The two main options we used were the normal and dense point cloud. The normal one gave a basic point cloud, whilst the dense one gave a coloured point cloud. These were very similar

to the results of the Pix4D software. For the 1st batch of pictures, 113.268 points were generated. In case of the dense point cloud, 16.200.785 points were generated.

Other present features include, but are not limited to: 3D model: generation and texturing, Spherical panorama stitching, Dense point cloud: classification, DEM: georeferenced DSM / DTM export, Georeferenced orthomosaic export, Orthomosaic seamline editing, Markers / scale bars support, Ground control points support, Coded / non-coded targets auto detection, Multispectral imagery processing and others. It is possible to export files in a .las format, which ensures easy transferability between programs.

The main downfall of this software package is the lack of some sort of quality report as can be obtained from Pix4D. Therefore, it isn't as fast and easy to represent and analyse the accuracy of the model generated through the pictures. (Agisoft, 2019)

10.2.2 User-friendliness

The interface and menus of this software solution are more cluttered than the other options. It lacks some of the functionality that the other software solutions provide. A quality report is not available, in contrast to the Pix4D and ARCGIS Drone2Map.

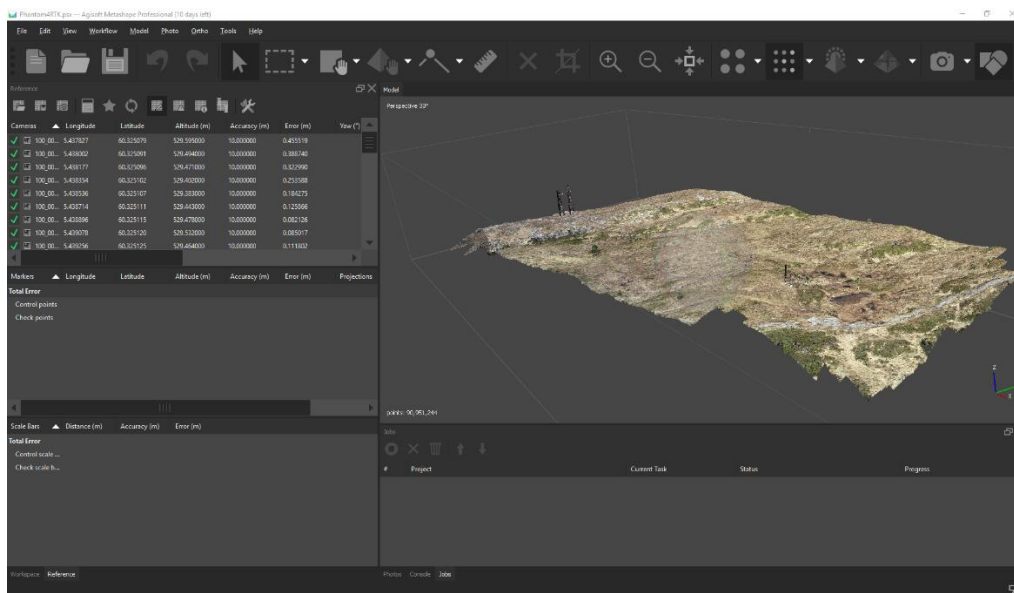


Figure 20 Agisoft Metashape Professional user interface (own image)

10.3 ARCGIS Drone2Map

10.3.1 Functionality

The options available are almost identical to the ones in Pix4D. There are options present for 2D renderings, for maps, 3D renderings, for inspection and or detailed models. The main difference is that instead of having to do the rendering in multiple steps like in Pix4D (first point cloud, afterwards things like DSM, DTM, rayCloud, meshes, etc..) you can select all of the desired outputs at once. This means that it can save a certain amount of time, because it is possible to render only the desired point cloud.



Figure 21 ARCGIS Drone2Map point cloud (own image)

In the 2D category, DSM and DTM models are available. An orthomosaic map can also be rendered. On each and every rendering, it is possible to see the flight plan and pictures taken from the drone. These maps are almost identical to renderings of Pix4D.

For 3D renderings, there are a multitude of options as well. The main option we focused on were the point clouds. It is possible to generate models specifically for inspection of 3D objects. You can also generate coloured meshes and dense coloured point clouds.

Similarly to Pix4D, there is also a function to obtain a detailed quality report. This can be viewed in the software, or exported in a .PDF format. All needed information about accuracy and variance is present in this document. For the first batch, it generated a dense point cloud of 13.862.737 points. This is very close to the amount generated by Pix4D. The second batch of pictures 21.278.414 points.

The last advantage Drone2Map offers is the option to transfer any data to ARCGIS instant, without having to use a specific file format and or do any kind of transfer. It is done at the press of one button.

10.3.2 User-friendliness

The software is easy and simple to use. The implementation of a larger amount of processing options is a definite advantage. Every function of the software is well documented and explained in the help function and the available ESRI forums. The layout makes every function easy to find and utilize.

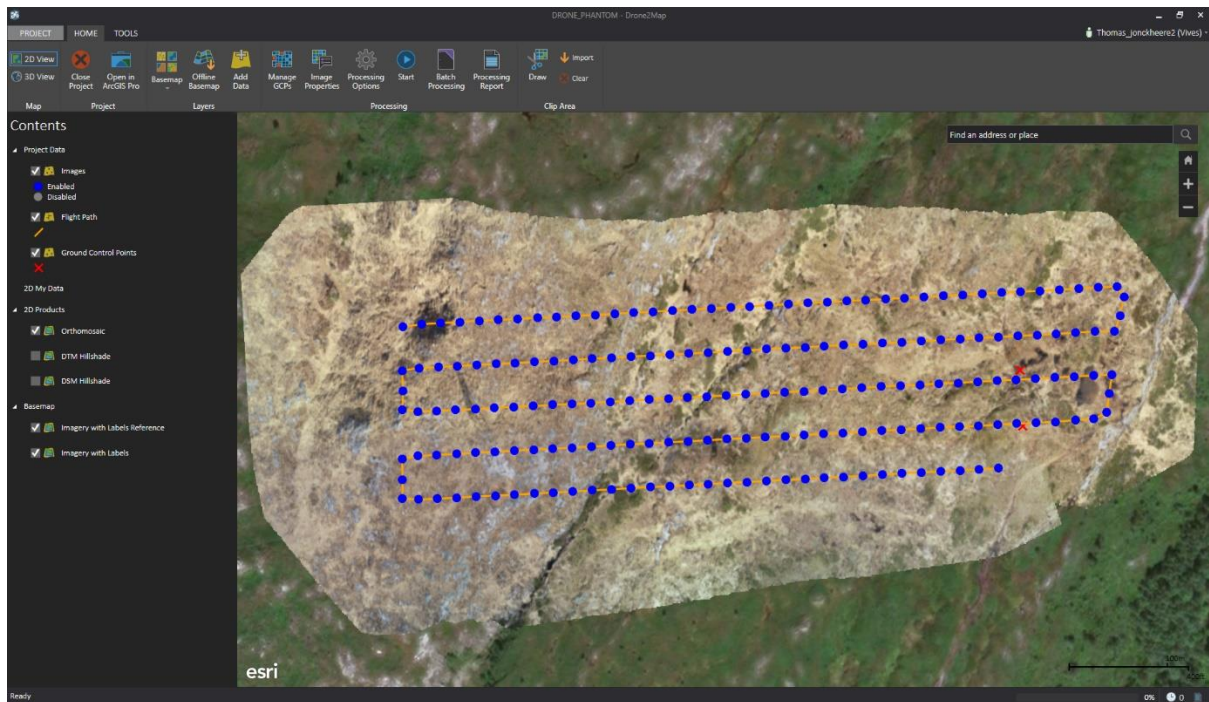


Figure 22 ARCGIS Drone2Map user interface (own image)

11 Theory

11.1 Navigation system

11.1.1 GNSS

GNSS is an umbrella term that covers all satellite navigation systems that give autonomous geo-spatial positioning with global coverage. So this means that this term also covers things like the Russian system GLONASS, GPS, Galileo,....

With a GNSS system you have the advantage of having connection to multiple satellites which results in a higher accuracy. Also, if one part of the GNSS system fails (doesn't happen often, but it can happen) the other receivers of GNSS can pick up the signal.

According to DJI their Phantom 4 RTK has a 1cm horizontal accuracy and a 1.5cm vertical accuracy (DJI, 2019).

11.1.2 GPS

GPS is the most well-known and the most used positioning system all around the world.

A full installation consists of 24 satellites, but in practise the system has access to up to 32 satellites around the orbit of the earth. These satellites are divided over six different orbital planes (Rieke, Foerster, Geipel, & Prinz, 2011).

According to DJI their Mavic Pro has an accuracy of less than 3metres (DJI, 2019).

11.1.3 RTK

An RTK GNSS in combination with an UAV has the potential to reach an accuracy of 1 to 3 cm (Rieke, Foerster, Geipel, & Prinz, 2011). Which is a lot better compared to that of a GPS without RTK (Van Sickle, 2008).

So the way a RTK works is that it receives signals of a global positioning system (GLONASS, SAPOS, ...) using a common modem. These signals are used to improve the positioning of the UAV.

So simply put: RTK is a system that is used to correct data collected from GNSS. Making the data more accurate.



Figure 23 RTK antenna on UAV (DJI, 2019)

To be able to receive the GNSS signals the UAV has to be equipped with an advanced dual-frequency GNSS antenna so it can receive and use all the available navigation signals. (Figure 23)

11.2 Photogrammetry

11.2.1 Introduction

In short: photogrammetry is the method that uses photography to measure distances.

11.2.2 How does it work?

If you have an object that is seen from two cameras from two different points of view, you can estimate its position. Your eyes are doing that all the time, that is why people with one eye have problems with estimating depth.

However, computers can use more than two points of view to construct a model, either to improve the accuracy or to construct a model that cannot be framed into a single pair of pictures.

Any kind of camera can be used for photogrammetry; from your smartphone to a professional digital camera or even specialized systems mounted on planes and even satellites.

With photogrammetry we can compute the position of objects that are seen on two or more images. If we cover a whole area with pictures, then we can compute a 3D model of the whole area. Using that, we can compute an orthoimage.

An orthoimage is an image that can be overlaid on a map. For instance: if you take pictures vertically above your book that is lying on your desk and move over it while taking pictures and you make sure that at least every corner and book cover is seen in two pictures. With these pictures you can create a 3D model. From this model you can extract the orthoimage.

The 3D formation allows the correct size for the difference in perceived size. For example, if you take a picture of a mountain with houses on it, the picture will show that the houses on the bottom of the mountain are smaller in comparison with the houses on the top. With an orthoimage, the houses are the same size.

11.2.3 When do we use photogrammetry?

We can use it to produce models of small archeologic artefacts or buildings or even to make a map of the whole country. The technique of photogrammetry is also used for making 3D movies.

11.2.4 How do we use it in geoscience?

3D models of volcanoes, for instance, are very useful to be able to understand how they move, how they change and even maybe predict eruptions. It is also used to see how landslides or glaciers are moving and sliding. You can also use it for topological mapping.

11.2.5 The important aspects.

Types of aerial photogrammetry

1. Aerial photograph and basic concept
2. Image scale
3. Photogrammetry measurement
4. What is the best overlap and how we come by it
5. How the software calculates the flight plan
6. Point cloud

1. Types of aerial photogrammetry

There are three types of aerial photogrammetry, namely vertical, low-oblique and high-oblique. In our survey we only used the vertical type, where the camera is pointed vertically to the ground surface (Figure 24).

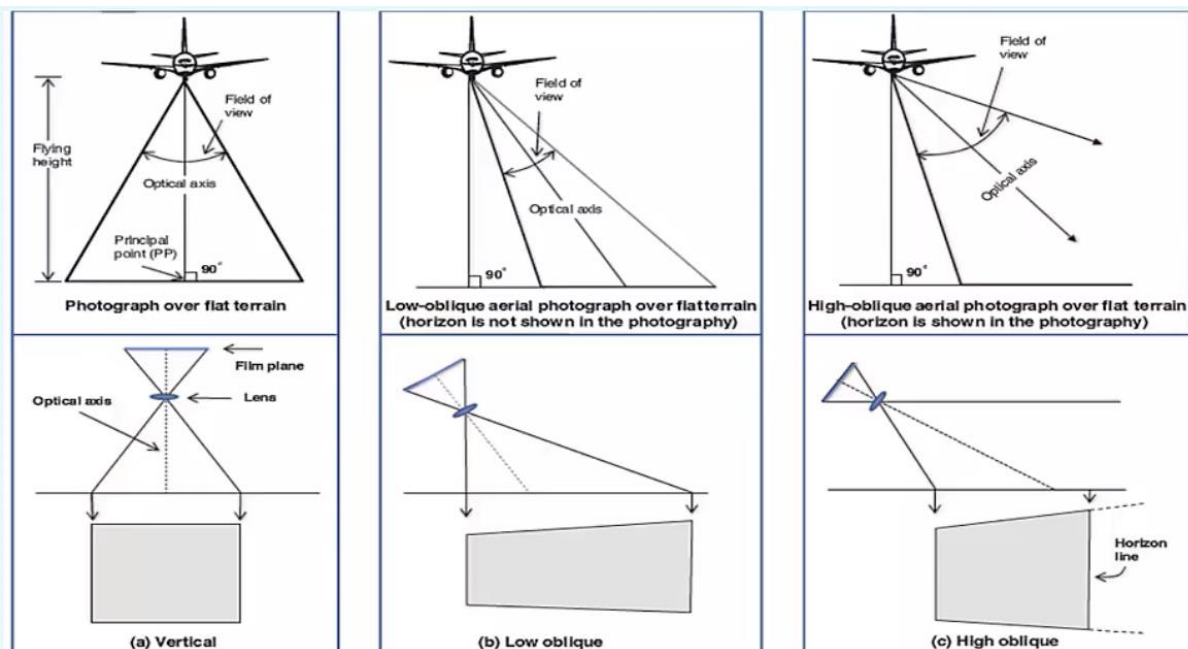


Figure 24: types of aerial photogrammetry (L. H. Nama, *An Approach for Coverage Path Planning for UAVs*, 2016).

2. Aerial photograph and basic concept

Important definitions of photogrammetry (Figure 25; Figure 26):

- Focal length (f): it defines the distance between the camera lens and the image plan, it shows the scale of area photograph.
- Flying height (H): this indicates the height of the aircraft above the ground.
- Fiducial marks: are the centre of four or five area photographs.
- Principal points (pp): this is the centre of the photograph, which also is the intersection of lines connecting to opposite fiducial marks. It is a point on the ground where the Optica axes of the camera points (Thomas M. Lillesand, 2004), (Charles D. Ghilani, 2012).

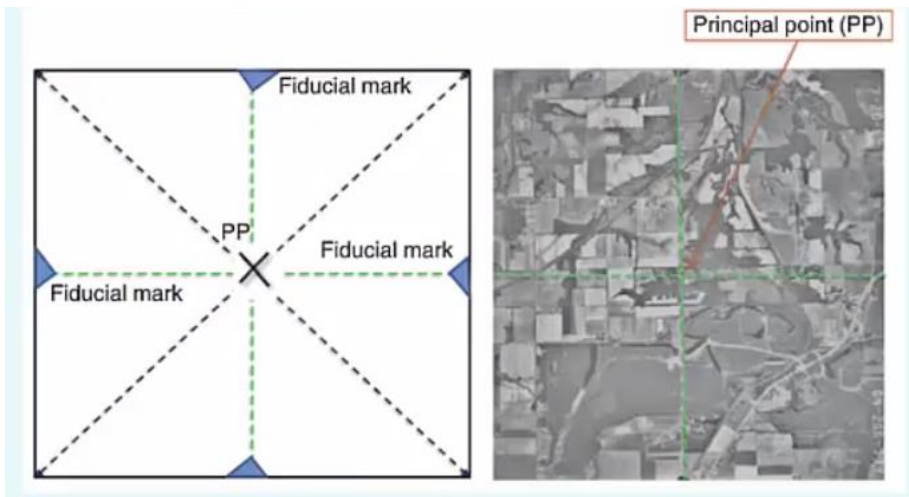


Figure 25 (L. H. Nama, *An Approach for Coverage Path Planning for UAVs*, 2016).

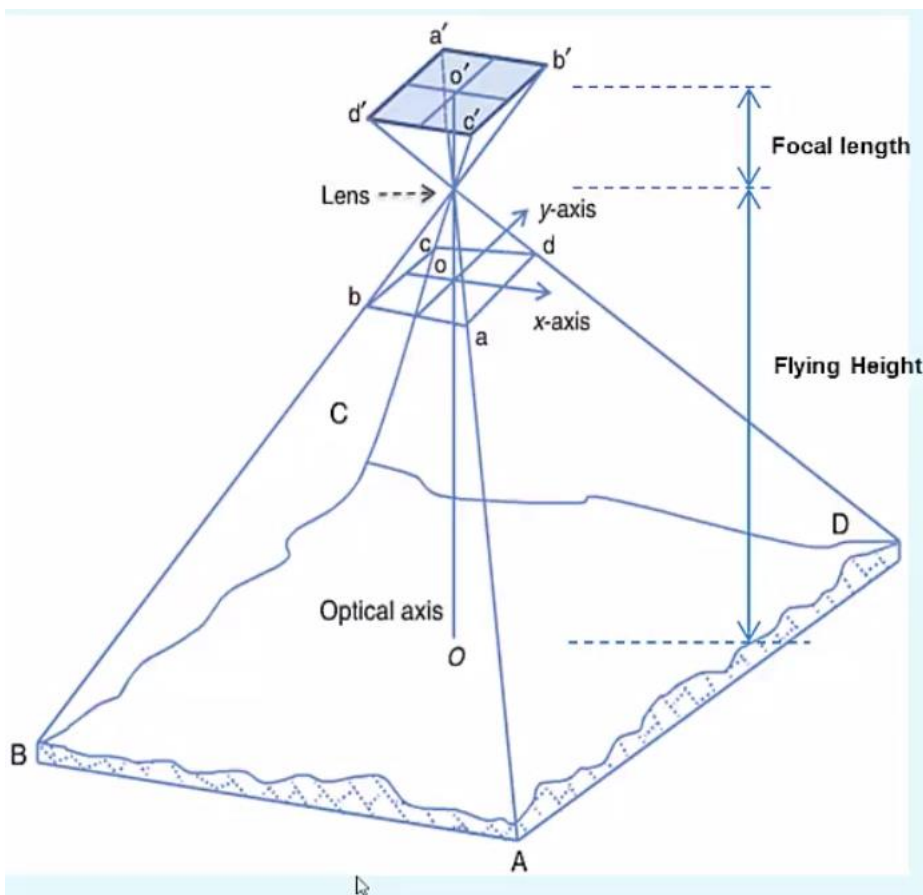


Figure 26 (Thomas M. Lillesand, 2004).

3. Image scale

It is the ration between the size of the object mirrored on the aerial photograph, compared to the actual size of the object in the real world (Thomas M. Lillesand, 2004), (Charles D. Ghilani, 2012).

- $s = \frac{S_i}{S_r}$
- s: image scale
- S_i : size of the object on the image
- S_r : size of the object in the real world

For example, the image scale is 1:10.000, this means that 1 mm on the image is 10.000 mm in the real world.

This equation scale can be defined as a ration between the focal length and flying height.

- $\text{Scale} = \frac{f}{H}$
- f: focal length
- H: flying height

If the image scale and focal length is given, then the flying height can be calculated (Figure 26)

4. Photogrammetry measurement

Given overlapping images, the height of the building above ground can be calculated (Figure 27).

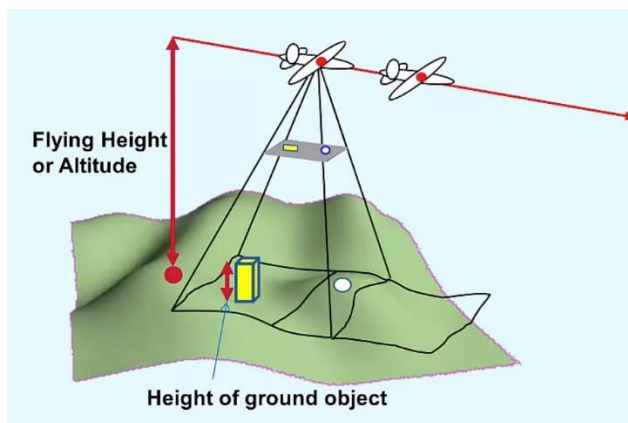


Figure 27 (Corke , 2012)

- Height measurement: $h = \frac{d \times H}{r}$
- d = relief displacement (for example, 20 pixels)
- H = flying height
- r = radial displacement (for example, 200 pixels)

d and H are the 2D measurements on the aerial photograph. These cover relief displacement of the image projection of the vertical building and r covers the radial displacement which is the distance of building top from the principal point (Figure 28) (Charles D. Ghilani, 2012), (Thomas M. Lillesand, 2004).

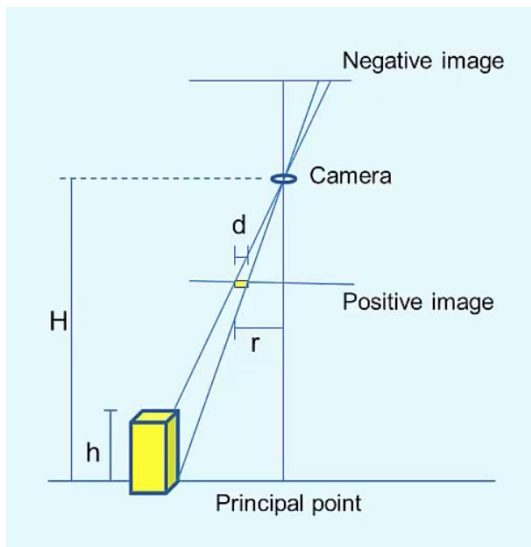


Figure 28 (Corke , 2012)

A. Parallax

Parallax is the displacement between two images of a 3D point. It is in relation with the distance and reversely proportional to the distance.

In Figure 29, the pencil is very displaced because it is close to the observer, the church is less displaced because it is further away.

The calculation of building height from a single image:

We need to measure distance between the top and bottom of the object. Sometimes it is hard to measure that accurately, due to the quality and resolution of the photograph. In this case we can also use another photogrammetry technique called a stereoscopy and measure a 3D object from a pair of overlapping area photographs.

What is the principle of stereoscopy? The parallax is the displacement of the 3D precision on two images caused by different positions of observation. It releases the 3D position of the object from the camera. The parallax is reversely proportional to the distance of 3D position from the camera, which means the larger the parallax, the closer the object in 3D from the camera (Thomas M. Lillesand, 2004), (Charles D. Ghilani, 2012).

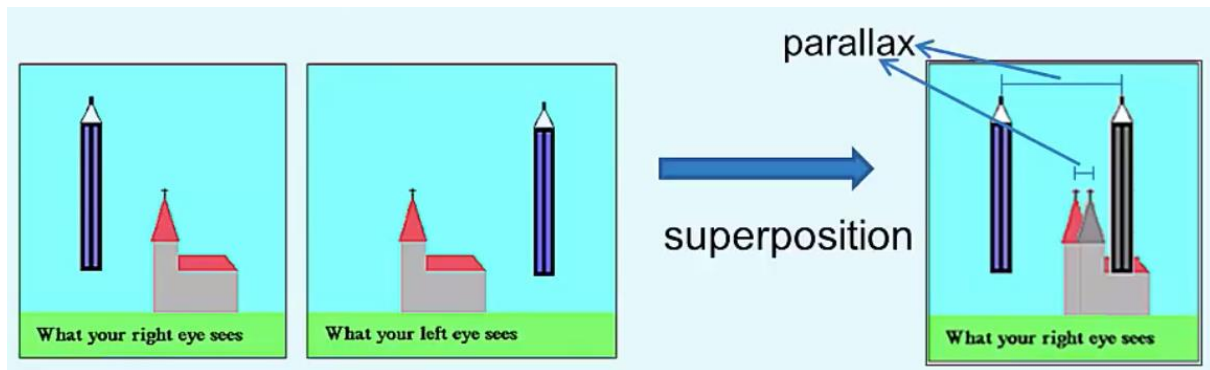


Figure 29 (Corke , 2012)

There are **two constants** we need to understand before we can do the 3D measurement by using the stereoscopy. The first one is called the absolute stereoscopic parallax; it is the photo distance between the principal point on one photograph and the responding principal point on the other photograph, also called the conjugated principal point. The second one is called the differential parallax. (Thomas M. Lillesand, 2004), (Charles D. Ghilani, 2012).

Absolute stereoscopic parallax (Figure 30)

- PP: principal point
- CPP: conjugate principal point = adjacent photo's principal point
- P : absolute stereoscopic parallax: the average distance between PP and CPP,
 $p = (p_1 + p_2) / 2$

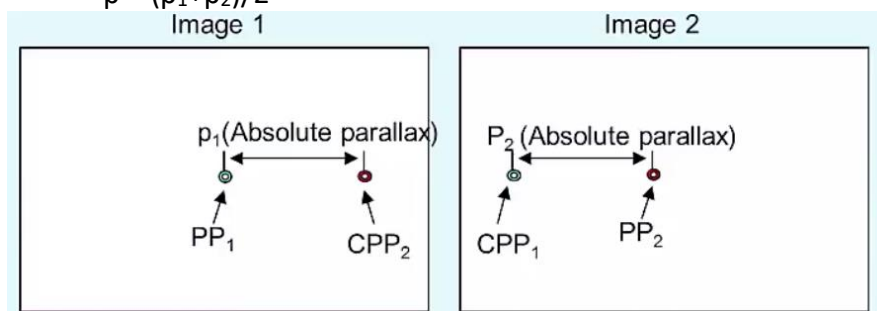


Figure 30 (Corke , 2012)

Differential Parallax (Figure 31).

- Differential parallax (dp) = the difference between the stereoscopic parallax at the top and base of the object, $dp = p_b - p_t$

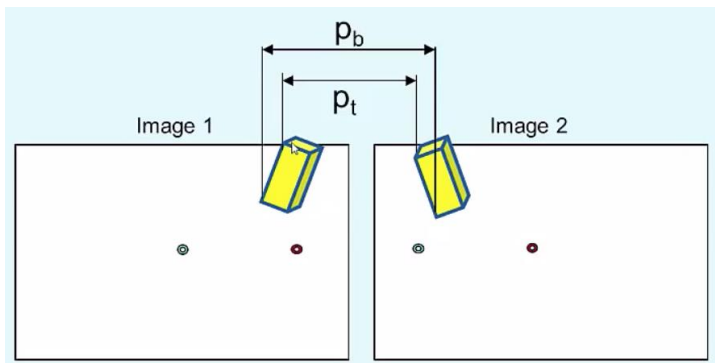


Figure 31 (Corke , 2012)

Equation of 3D measurement

- $h = H \frac{dp}{p+dp}$
- H: flying height
- dp: differential parallax (for example, 15 pixels)
- p: absolute parallax (for example, 90 pixels)
- h: is the height of the building or object

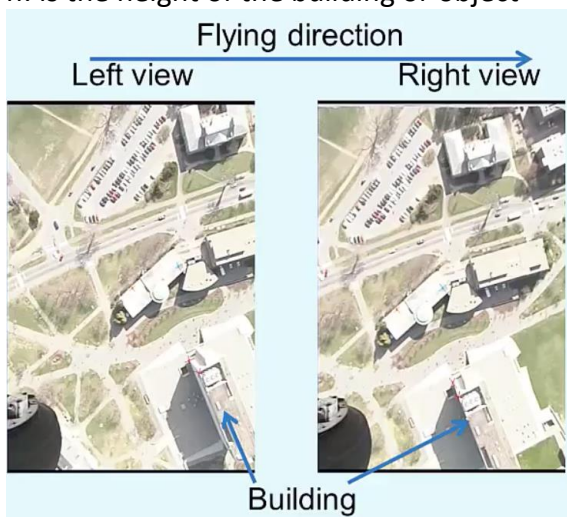


Figure 32 (Corke , 2012)

5. What is the best overlap and how we come by it

PHOTO OVERLAP

Aerial photo projects for all mapping and most image analyses require that a series of photos must be taken alongside each of the multiple flight lines. To make sure of stereoscopic coverage throughout the site, the photographs must overlap in two directions: in the line of flight and between adjacent flights (Dennis Morgan, 2001).

A. End-lap

End-lap or forward overlap is the common image area on consecutive photographs along a flight strip. This overlapping area of two successive aerial photos, which you need to create the 3D effect necessary for mapping, is known as a stereomodel or more known in general as

a “model.” Figure 33 shows the End-lap area on a single pair of consecutive photos in a flight line.

All projects need more than a single pair of photographs. Usually, the aircraft follows a predetermined flight line as the camera exposes successive overlapping images (Dennis Morgan, 2001).

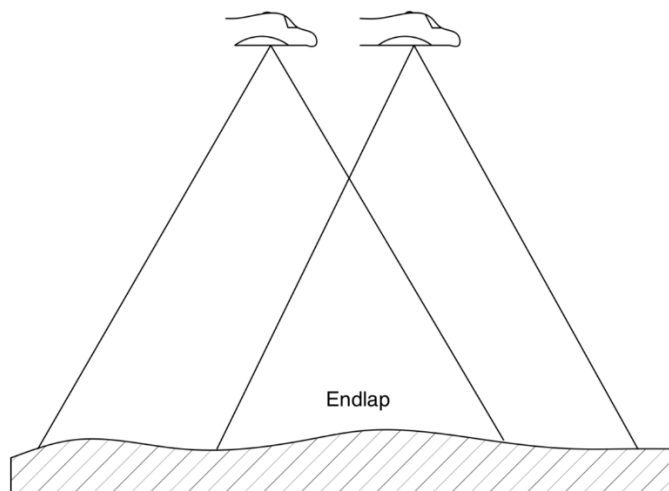


Figure 33 End-lap on two consecutive photos in a flight line (L. H. Nama, *An Approach for Coverage Path Planning for UAVs*, 2016).

In most cases the end-lap ranges between 55% and 65% of the length of a photo, with a nominal average of 60% for most mapping projects, we used an end-lap of 80%.

End-lap gain, the distance between the centres of consecutive photographs along a flight path, can be calculated by using equation g_{end} (Dennis Morgan, 2001).

$$g_{end} = s_p * w * \left[\frac{(100 - o_{end})}{100} \right]$$

where:

g_{end} = distance between exposure stations (feet)

s_p = photo scale denominator (feet)

o_{end} = endlap (percent)

w = width of exposure frame (inches)

When using a precision aerial mapping camera with a 9 × 9 inch exposure format and a normal end-lap of 60%, this makes the formula simpler. In this case, two of the variables become constants (Dennis Morgan, 2001):

$w = 9\text{inch}$.

$O_{end} = 60\%$

Then, the expression $w * [(100\% - O_{end})/100]$ becomes a constant equal to 3.6, and equation g_{end} may be supplanted by the equation of q_{end} (Dennis Morgan, 2001).

$$q_{end} = s_p * 3.6$$

When using a camera other than a 9 × 9 inch format and/or an end-lap other than 60%, the equation of g_{end} must be used (Dennis Morgan, 2001).

B. Side-lap

Side-lap or side overlap includes the overlapping areas of photographs between adjacent flight lines. The programme is designed so that there are no gaps in the 3D coverage of a multiline project. Figure 34 shows the relative head-on position of the aircraft in adjacent flight lines and the resultant area of exposure coverage (Dennis Morgan, 2001).

Normally, the side-lap ranges between 20% and 40% of the width of a photo, with a nominal average of 30%. Figure 34 portrays the side-lap pattern in a project requiring three flight lines (Dennis Morgan, 2001).

Side-lap gain, the distance between the centres of adjacent flight lines, can be calculated by using equation g_{side} (Dennis Morgan, 2001).

$$g_{side} = s_p * w * [(100 - o_{side})/100]$$

where:

- g_{side} = distance between flight line centers (feet)
- s_p = photo scale denominator (feet)
- o_{side} = sidelap (percent)
- w = width of exposure frame (inches)

When employing a precision aerial mapping camera with a 9 × 9 inch exposure format and a normal side-lap of 30%, this makes the formula simpler. Then, two of the variables become constants (Dennis Morgan, 2001):

$$w = 9 \text{ inch}$$

$$O_{side} = 30\%$$

Therefore, the expression $w * [(100\% - O_{side})/100]$ becomes a constant equal to 6.3, and equation g_{side} may be supplanted by equation q_{side} (Dennis Morgan, 2001).

$$q_{side} = s_p * 6.3$$

When using a camera other than a 9 × 9 inch format and/or a side-lap other than 30%, equation g_{side} must be employed (Dennis Morgan, 2001).

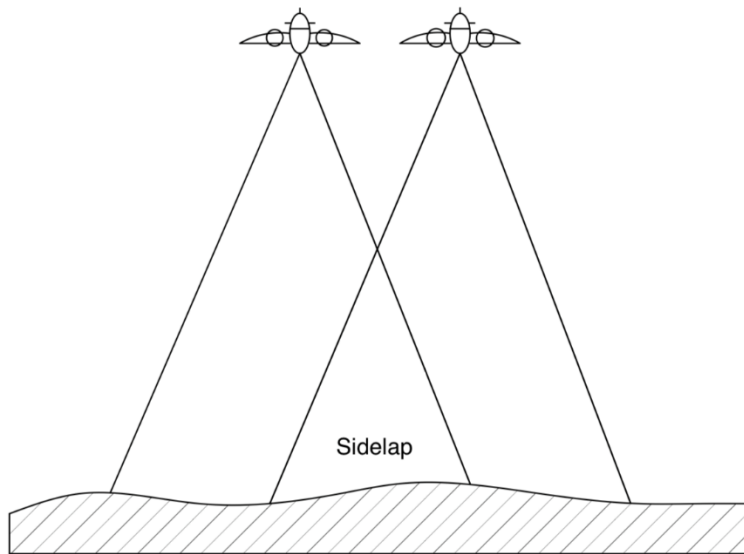


Figure 34 Side-lap between two adjacent flight lines (L. H. Nama, An Approach for Coverage Path Planning for UAVs, 2016).

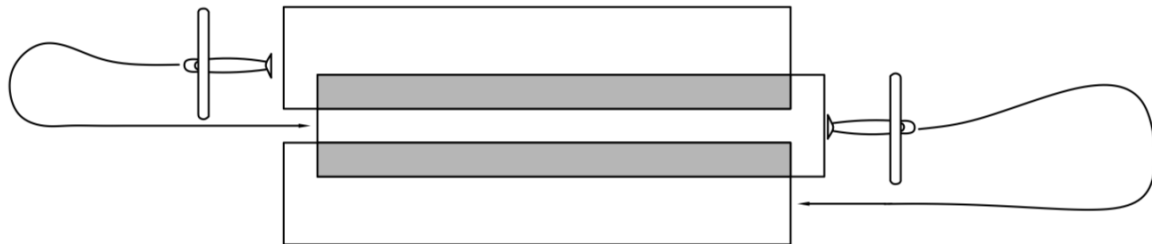


Figure 35 Side-lap on three adjacent flight lines (L. H. Nama, An Approach for Coverage Path Planning for UAVs, 2016).

C. Stereomodel

From the previous part of overlap, it is evident that consecutive photos in a flight strip overlap. When focusing each eye on a particular image feature that was viewed by the camera from two different aspects, the mind of the observer is convinced that it is seeing a lone object with three dimensions. Put simply, the 3D effect is an optical illusion. This phenomenon of observing a feature from different positions is known as the parallax effect. Although used to describe other facets of photogrammetry, parallax is defined as a change in the position of the observer. In this situation the viewer, when using appropriate stereoscopic instruments to observe a pair of 2D photos, can see a single 3D image (Dennis Morgan, 2001).

Photogrammetrists envision a model as the “clean” area that a single stereopair contributes to the total project. This model generates an end-lap and side-lap with surrounding photos. A mapping model is shown as the crosshatched area in Figure 36 (Dennis Morgan, 2001).

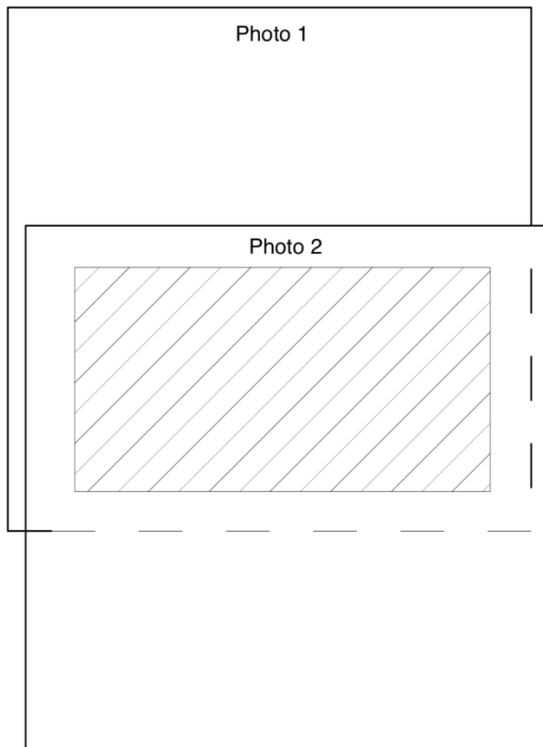


Figure 36 clean area of a stereomodel (L. H. Nama, *An Approach for Coverage Path Planning for UAVs*, 2016).

The important thing to realize is that the scale of individual photographs in a project is not a constant. Due to undulations in the aircraft flight and terrain relief, the distance between the camera and the ground changes from one exposure to another. Therefore, you must consider the scale of the photo as an average scale for the total project (Dennis Morgan, 2001).

6. How to get the route of the drone or the UAV

In a survey assignment, one of the most important tasks of the flight planner is to generate the UAV's (unmanned aerial vehicle) path to completely cover the area of interest efficiently and it is tackled with the coverage path planning (CPP) technique. CPP is a sub-topic of motion planning for robots and uses methods to determine a path that ensures complete coverage while avoiding obstacles.

The CPP can accomplish verifiable coverage guarantee by using cell decomposition. A cell decomposition breaks down the target region into cells that can be covered easily. The complete coverage is accomplished by ensuring that the robot goes to each cell once. The workplace is generally mapped in exact cellular decomposition or approximate cellular decomposition (L. H. Nama, *An Approach for Coverage Path Planning for UAVs*, 2016).

The exact cellular decomposition method develops from the trapezoidal decomposition, in which each cell's shape is a trapezoid. Simple back-and-forth movement can be used to cover each cell. The downside of this method is that the UAV's camera field of view (FOV) is neglected. This can lead to high overlapping in coverage, thus reduces the efficiency of the UAV survey. To solve the problem, scientists (Y. Li, *Coverage path planning for UAVs based on*

enhanced exact cellular decomposition method,, 2011) proposed an enhanced exact cellular decomposition method to plan the coverage path of UAVs in a polygon area. An algorithm to calculate the widths of convex polygons is developed and a path of the least number of turns for an UAV based on the width of the convex polygons is developed. Better results in path planning were obtained by avoiding unnecessary back and forth motions. However, the camera's FOV is still neglected (L. H. Nama, An Approach for Coverage Path Planning for UAVs, 2016).

An approximate cellular decomposition of CPP for UAVs in agriculture application was introduced (J. Valente, 2013). An approximate cellular decomposition is a grid-based representation of the working area. Each cell has the same size and shape, and the union of the cells approximates the target region. The cell size is determined by the camera's FOV. When the robot visits each cell's centre in the decomposition, the coverage is complete. The path of the robot can be determined through spanning trees, neural networks, genetic algorithms, and general heuristic search algorithms. The approximate cellular decomposition combined with wavefront algorithm with gradient ascent can be used to determine the coverage path with a minimal number of turns (J. Valente, 2013). In addition, the so-called Pedestrian Pocket Algorithm (PPA) based on the backtracking method can be used to find near optimal path and Quad Tree Algorithm can be used to reduce the computation time. To make the UAV return to the base station before it is out of power, the shortest return path for the UAV is computed using wavefront algorithm with the steepest gradient descent method. However, in this case, the criteria of the minimum number of turns is no longer relevant to the path planning as it may lead to longer travelling distance. At this stage, the flight planner is only required to input a set of waypoints to the UAV's built-in auto pilot to generate a smooth trajectory for the UAV to follow (L. H. Nama, An Approach for Coverage Path Planning for UAVs, 2016).

A. Wavefront algorithm

The navigation function $\phi: G \rightarrow [1, \infty]$ has the same feature as a potential function. For the goal cell, the navigation cost $\phi(c_G) = 1$ and the further the cell position to the goal cell, the larger the navigation cost. The waypoint u^* , which is at the adjacent cell of the current way point x , can be selected to reduce the potential as much as possible (gradient descending) or increase the potential as much as possible (gradient ascending) (L. H. Nama, An Approach for Coverage Path Planning for UAVs, 2016).

Gradient descending $u^* = \operatorname{argmin}\{\phi(u)\}, u \in U(c)$

Gradient ascending $u^* = \operatorname{argmax}\{\phi(u)\}, u \in U(c)$

Where:

c : current cell

$U(c)$: set of adjacent cells of c

u^* : next cell in path planning

The gradient descending searching algorithm is commonly used in robot path planning to find the shortest path from the start cell to the goal cell. For the coverage planning, the gradient ascending searching algorithm should be adopted where all the cells with higher value than the goal cell are guaranteed to be visited before the robot reaches the goal.

The navigation function can be established with the wavefront propagation algorithm, which is as follows (L. H. Nama, An Approach for Coverage Path Planning for UAVs, 2016):

1. Initialize $W_0 = c_G$; $\phi(c_G) = 1$
2. Initialize $W_{i+1} = \emptyset$.
3. For every $c \in W_i$, assign $\phi(c) = i$ and insert all unexplored neighbors of x into W_{i+1}
4. If $W_{i+1} = \emptyset$, then terminate; otherwise, let $i=i+1$ and go to step 2.

In order to construct a navigation function, we must consider the type of cell connectivity based on the manoeuvrability of the robot. There are two types of connectivity: the Von Neumann neighbourhood (Figure 37a) and the Moore neighbourhood (Figure 37b). In a Von Neumann neighbourhood, the aerial robot turning angle is limited to $\pm 90^\circ$. In the Moore neighbourhood, the robot will be able to turn $\pm 45^\circ$, $\pm 90^\circ$, or $\pm 135^\circ$. For a quad-rotors UAV, it can rotate to any yaw angle value by changing the velocity of all motors. Therefore, the Moore neighbourhood is chosen (L. H. Nama, An Approach for Coverage Path Planning for UAVs, 2016).

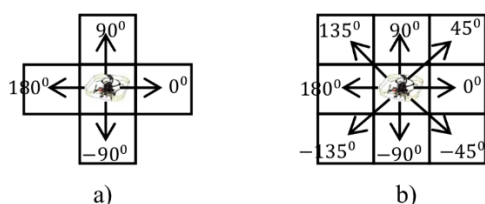


Figure 37 a) Von Neumann neighbourhood b) Moore neighbourhood (L. H. Nama, An Approach for Coverage Path Planning for UAVs, 2016)

During the gradient tracking, the algorithm may find more than one neighbour with the same potential. The unexpanded nodes or intersection points need to be recorded and labelled as a state of bottleneck. The bottleneck is a state caused by the local minimal during the search. In this case, the current searching path cannot completely cover the working area. A new search needs to be started from the unexpanded nodes. Hence, a backtracker needs to be implemented to record the unexpanded nodes. The result of this gradient ascending searching algorithm is a set of waypoints that will ensure complete coverage. All waypoints contain information about x , y and yaw angle φ .

As a result of path planning in the grid-based environment, the survey path comprises of multiple straight segments with different angles as shown in Figure 38. Therefore, it is assumed that the UAV will move with maximum velocity in straight lines, stop for rotating at the end of one straight segment and continue to move towards the next segments. The amount of time to complete the path can be calculated (L. H. Nama, An Approach for Coverage Path Planning for UAVs, 2016):

$$T = \frac{S}{V} + \sum_{i=1}^k \frac{\varphi_i}{\omega}$$

where

T : completion time

S : route length

V : UAV movement speed

k : number of turns

φ_i : angle of the i^{th} turn

ω : UAV rotation rate

An optimal path will be chosen to minimize the task completion time (Figure 38).

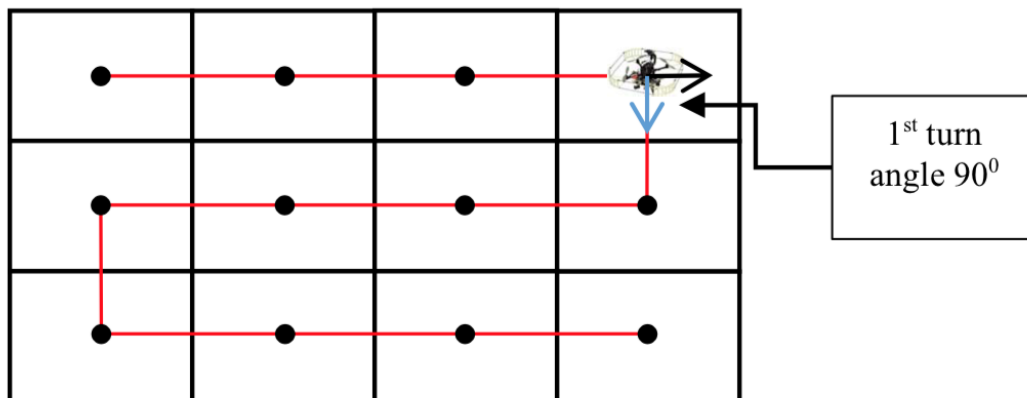


Figure 38 (L. H. Nama, An Approach for Coverage Path Planning for UAVs, 2016)

7. Point cloud

Photogrammetric point clouds utilize an algorithm to calculate corresponding points from pictures to form a 3D point cloud.

Neighbouring pictures are put into a grid, in which corresponding pixels are calculated. The pictures get transformed on top of each other, and each point is projected. If there are enough pixels that are found to be part of one projection, a point is generated in the point cloud (Figure 39). More overlapping pixels means that a more accurate representation of the point will be generated (Hodler, Visual and Statistical Comparisons of Surface Modeling Techniques for Point-based Environmental Data, 14 Mar 2013).

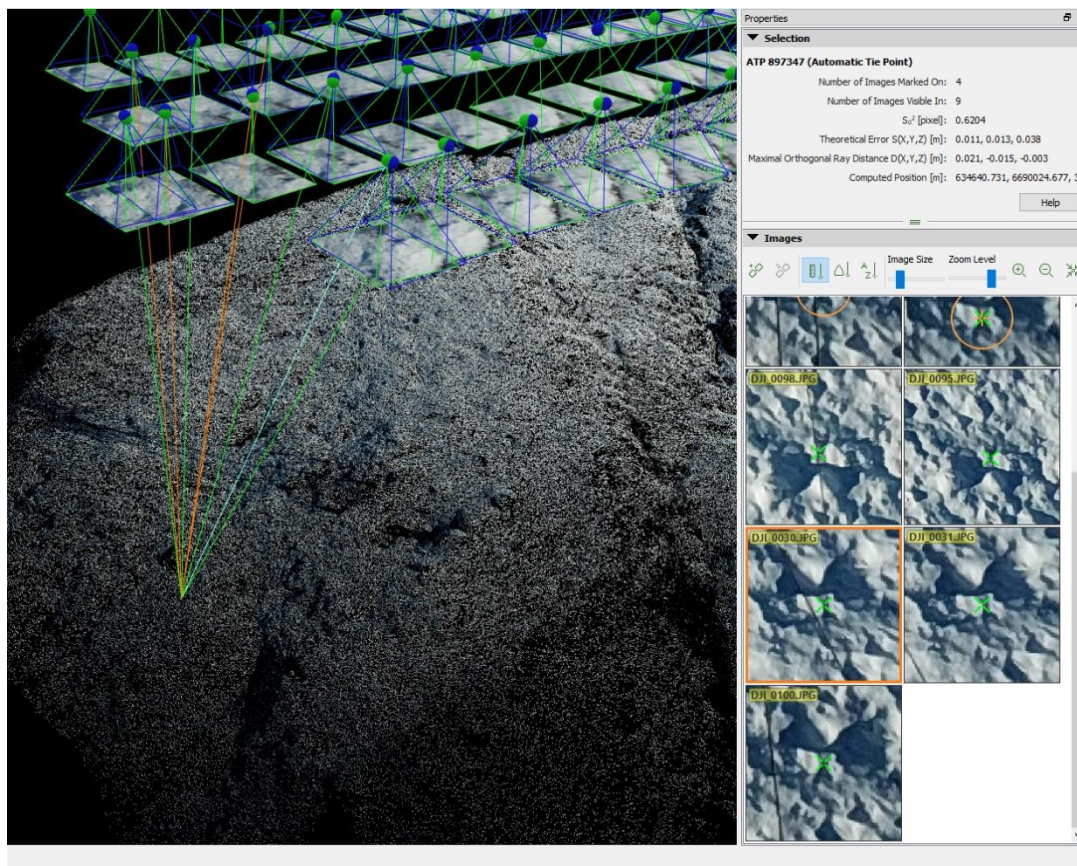


Figure 39: a single point projected out of 4 images (own image)

12 Results

12.1 General results

For the analysis of the results, we opted to look at the processed data from Pix4D. We decided to do this because Agisoft's reports didn't have the details we required, and Drone2Map didn't include the geolocation data from the RTK system of the Phantom4RTK drone. The QR reports of Pix4D cover all parameters we needed. All of the reports are included in the appendix of this report. Each drone has one report for each software solution we used.

For the inaccuracies of the processing itself, a general rule of thumb is taking the GSD and multiplying this by 3 (Pix4D, 2018). These are the uncertainties that are induced by the algorithm creating the point cloud.

These inaccuracies of the software are relative inaccuracies. What this means is, the error is relative to each point in the point cloud and not to the world. The relative inaccuracies can be measured through measuring an object with known length and depth in the generated point cloud. For this project, we used one of the concrete foundation blocks.

Table 1 Influence of GSD on general accuracy after processing (own table)

	Mavic PRO	Phantom 4RTK	Phantom 4RTK 50m
GSD (cm)	1,78	1,77	1,62
Inaccuracy of the pointcloud	5,34	5,31	4,86

Other important inaccuracies are the geolocation inaccuracies, these are called absolute inaccuracies. These are the errors in relation to the geolocation (the world). Each point that is in the point cloud has a geocoordinate with an x, y and z value that is in relation with WGS. The difference in position with the point in the point cloud and the geocoordinate is called the absolute inaccuracy. The accuracy depends on the used GNSS systems.

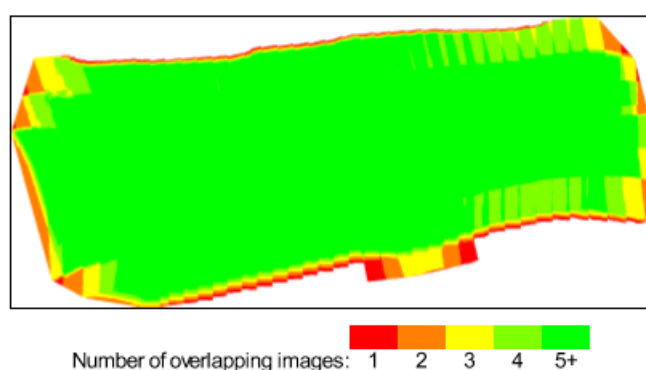


Figure 40 Image overlapping from MavicPro drone (own image)

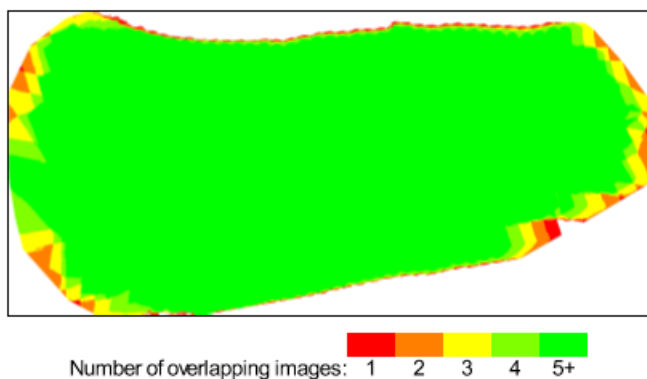


Figure 41 Image overlapping from Phantom4RTK drone (own image)

	Pix4D		Agisoft Metashape Professional		ARCGIS Drone2Map*	
	DJI MavicPRO	DJI Phantom4RTK	DJI MavicPRO	DJI Phantom4RTK	DJI MavicPRO	DJI Phantom4RTK
Processing Time						
Initial	1h38min	2h35min	1h40min	22h49min	2h14min	32min
Further processing	1h05min	1h43min	40min	2h58min	52min	1h21min
Processing load						
CPU usage (average)	89,00%	87,00%	88,00%	87,00%	91,00%	90,00%
RAM usage (average)	7,1 GB	7,0 GB	6,9 GB	6, GB	7,1 GB	7 GB

Figure 42 Processing time and load per software solution (own image)

*: Due to memory limitations on our processing computer, the quality of this render had to be significantly limited, because of LOD (Level Of Detail) memory errors. Therefore, we heavily recommend not to render these point clouds on computers with less than or equal to 8 GB RAM.

Table 2 Errors of measured points from the laserscanning data (own table)

	X	Y	Z
Point 1	0,040	0,001	0,014
Point 2	0,001	0,022	0,023
Point 3	0,030	0,028	0,007
Point 4	0,005	0,010	0,027
Point 5	0,000	0,000	0,000
Point 6	0,016	0,091	0,014
	Average =		0,018

Table 3 Relative uncertainties calculated from concrete foundation (own table)

Name		Y	X	Z	Line	Length
Measured foundation	T4	303648,044	6692863,012	441,322	T4 - T5 X	0,545
	T5	303648,070	6692862,467	441,321	T5 - T6 Y	0,593
	T6	303648,663	6692862,463	441,316	T6 - T7 X	0,760
	T7	303652,252	6692863,223	441,325	T6 - T7 Y	3,589
Phantom4RTK GCP		Y	X	Z	Line	Length
	T4	303648,080	6692863,060	441,340	T4 - T5 X	0,500
	T5	303648,010	6692862,560	441,340	T5 - T6 Y	0,670
	T6	303648,680	6692862,510	441,500	T6 - T7 X	0,690
	T7	303652,210	6692863,200	441,320	T6 - T7 Y	3,530
Length differences	Line	Δl				
	T4 - T5 X	0,045				
	T5 - T6 Y	0,077				
	T6 - T7 X	0,070				
	T6 - T7 Y	0,059				
Mean differences	Results					
Mean Δl	0,063					
Calculated GSD	0,049					
Difference mean GSD	0,014					

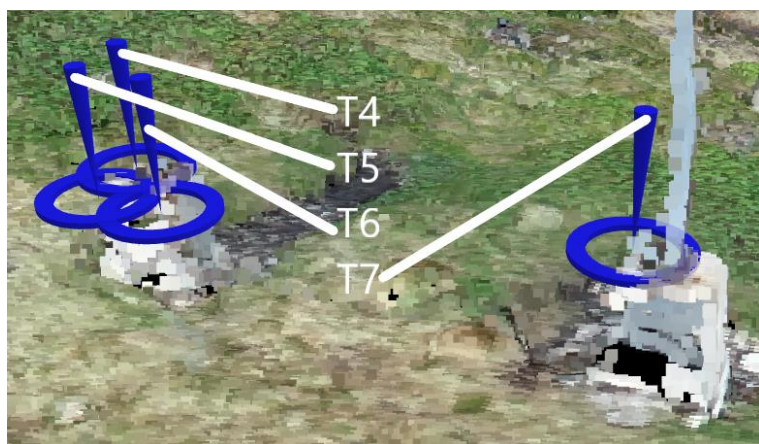


Figure 43 Known points on concrete foundation

Table 4 Absolute geolocation variance Phantom4RTK (own table)

Absolute geolocation variance Phantom4RTK						
M in Error [m]	Max Error [m]	Geolocation Error X [%] Phantom	Geolocation Error Y [%] Phantom	Geolocation Error Z [%] Phantom		
-0,03	-0,03	0,00	0,00	0,00		0,00
-0,02	-0,02	0,00	0,00	0,00		0,00
-0,02	-0,01	0,00	0,00	0,00		2,12
-0,01	-0,01	0,53	1,06			7,94
-0,01	0	46,56	46,56			14,80
0	0,01	52,38	52,38			23,28
0,01	0,01	0,53	0,00			26,46
0,01	0,02	0,00	0,00			16,93
0,02	0,02	0,00	0,00			4,76
0,02	0,03	0,00	0,00			2,12
0,03		0,00	0,00			1,06
		0,00	0,00			0,53
Mean [m]		-0,000015	0,000012			-0,00002
Sigma [m]		0,001951	0,00204			0,009121
RMS Error [m]		0,001951	0,00204			0,009121

Table 5 Absolute geolocation variance MavicPRO (own table)

Absolute geolocation variance MavicPRO						
M in Error [m]	Max Error [m]	Geolocation Error X [%] Mavic	Geolocation Error Y [%] Mavic	Geolocation Error Z [%] Mavic		
	-15	0,00	0,00	0,00		0,00
-15	-12	0,00	0,00	0,00		0,00
-12	-9	0,00	0,00	0,00		0,00
-9	-6	0,00	0,00	0,00		0,00
-6	-3	0,00	0,00	0,00		0,00
-3	0	58,27	49,64			46,76
0	3	41,73	50,36			53,24
3	6	0,00	0,00			0,00
6	9	0,00	0,00			0,00
9	12	0,00	0,00			0,00
12	15	0,00	0,00			0,00
15		0,00	0,00			0,00
Mean [m]		0	0			0
Sigma [m]		0,202405	0,34045			0,278153
RMS Error [m]		0,202405	0,34045			0,278153

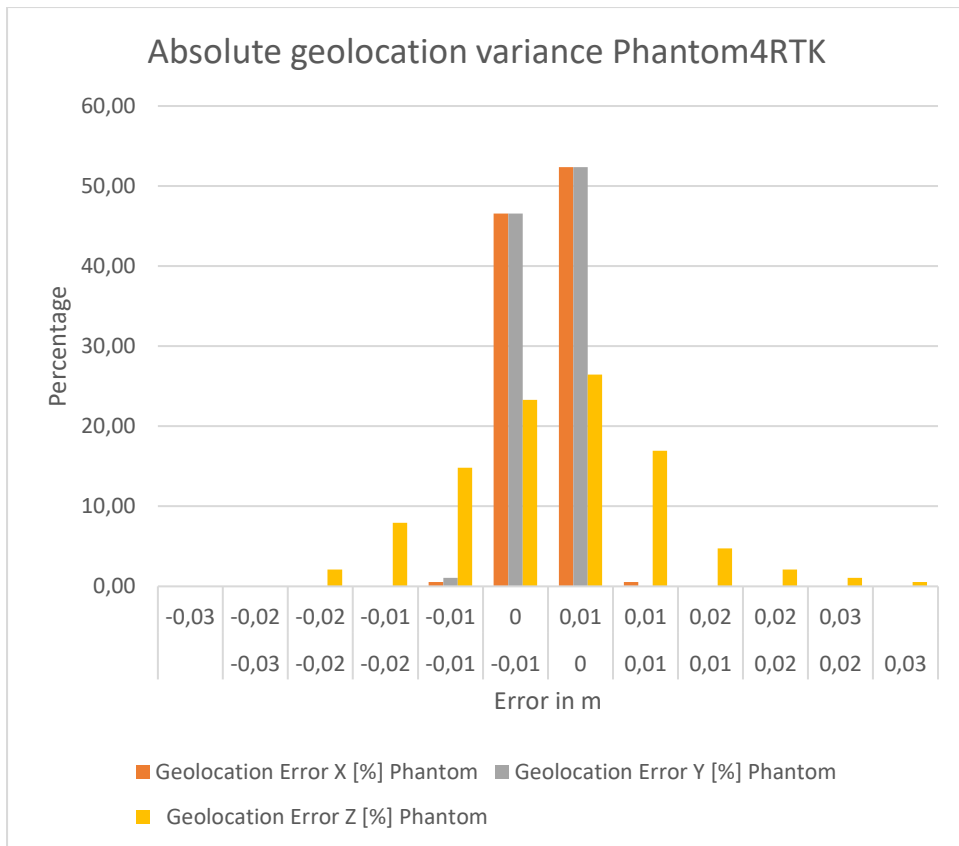


Figure 44 Graph of the absolute geolocation variance of the Phantom4RTK drone (own table)

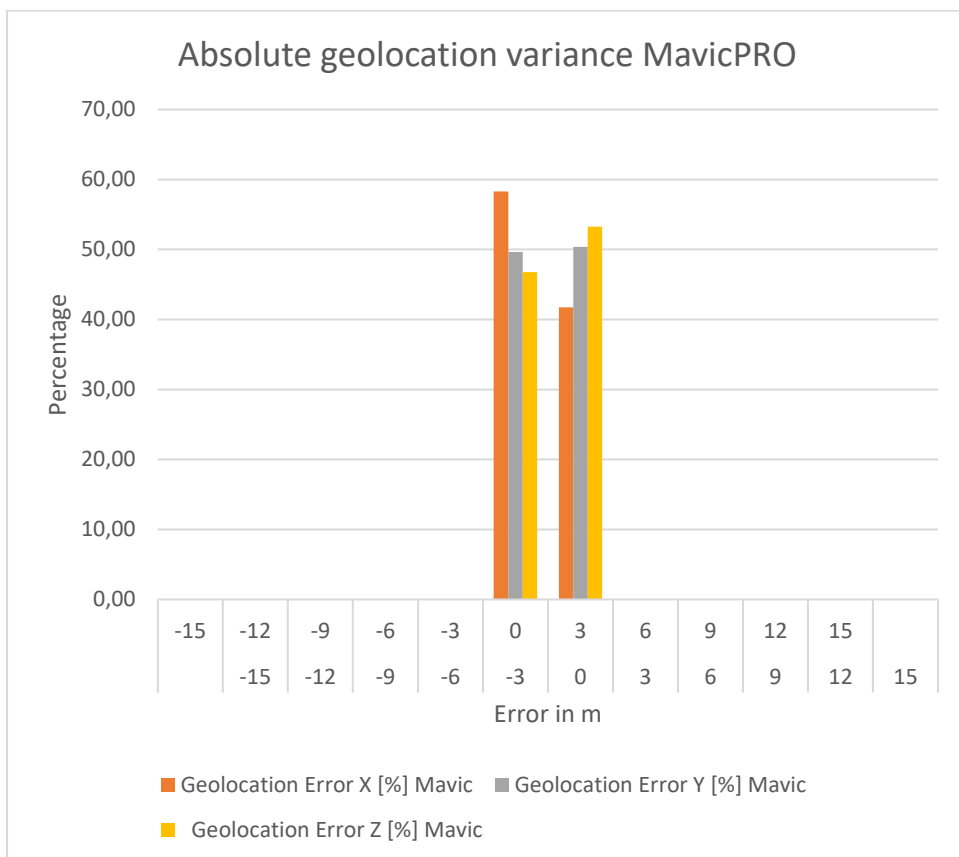


Figure 45 Graph of the absolute geolocation variance of the MavicPRO drone (own table)

Table 6 Calculation of translation (own table)

Name	X	Y	Z
Measured in Pix4D	303649,04	6692862,55	484,62
Measured GCP	303648,07	6692862,467	441,321
ΔXYZ	0,97	0,08	43,30

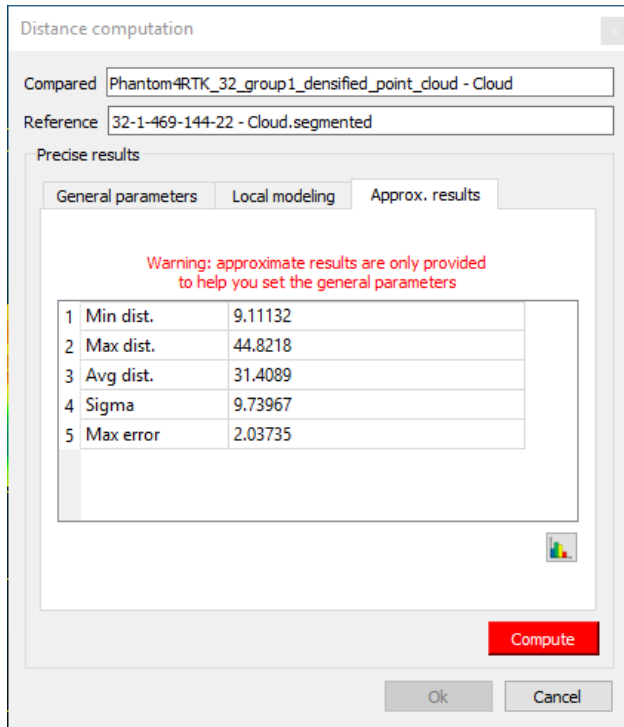


Figure 46 Distance computation between Høydedata and original Phantom4RTK point cloud in m (own image)

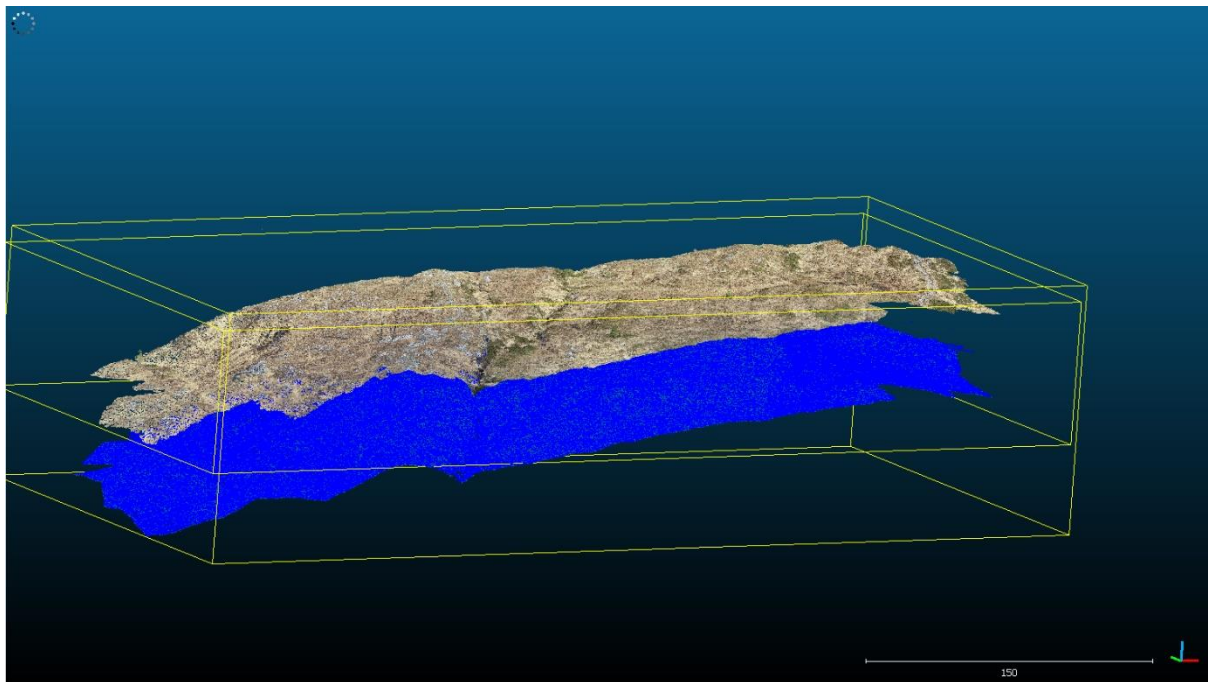


Figure 47 Cloud2Cloud distance Høydedata and original point cloud (own image)

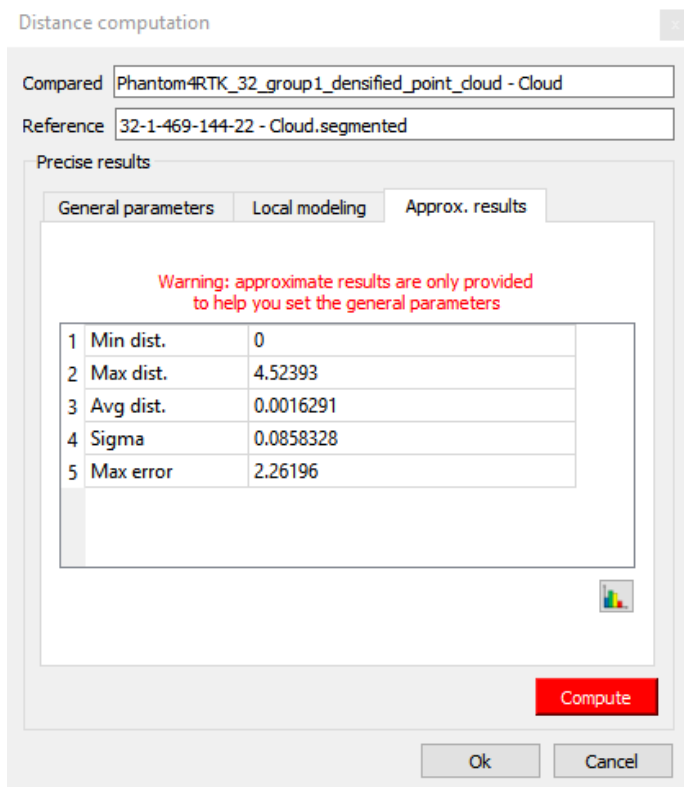


Figure 48 Distance computation between Høydedata and translated Phantom4RTK point cloud in m (own image)

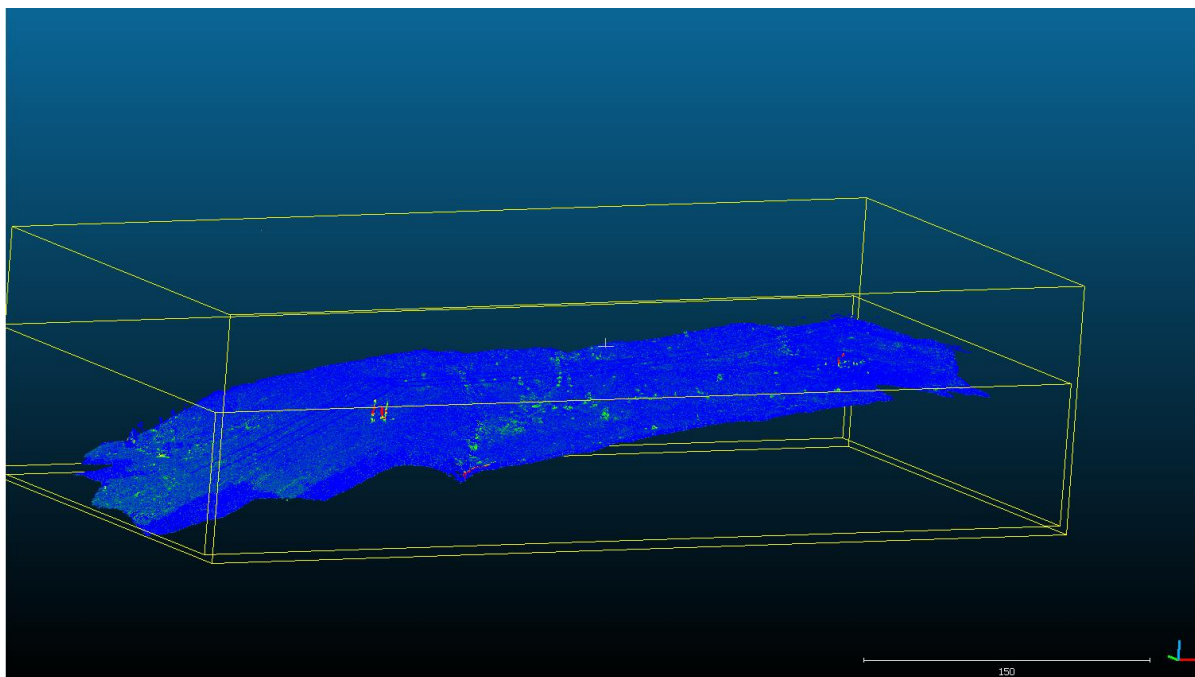


Figure 49 Cloud2Cloud distance Høydedata and translated point cloud (own image)

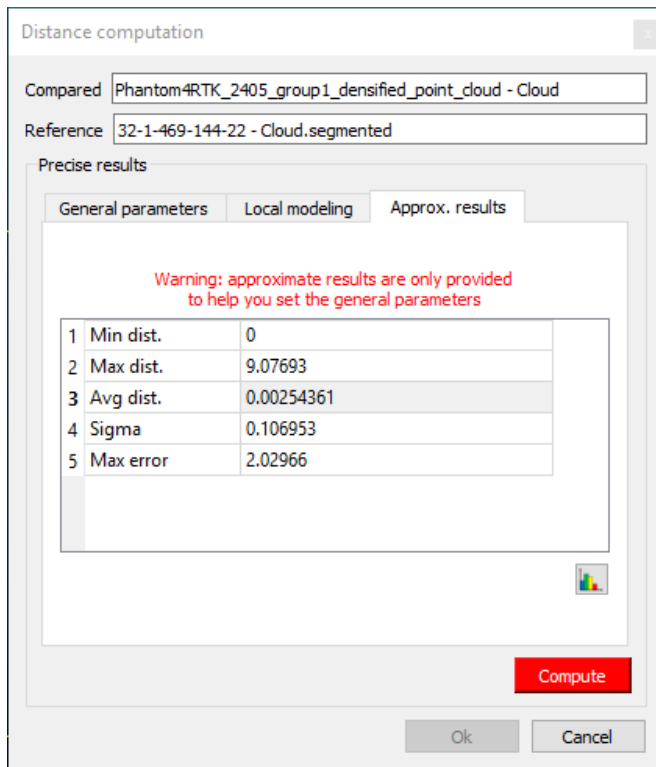


Figure 50 Distance computation between Høydedata and the GCP registered Phantom4RTK point cloud in m (own image)

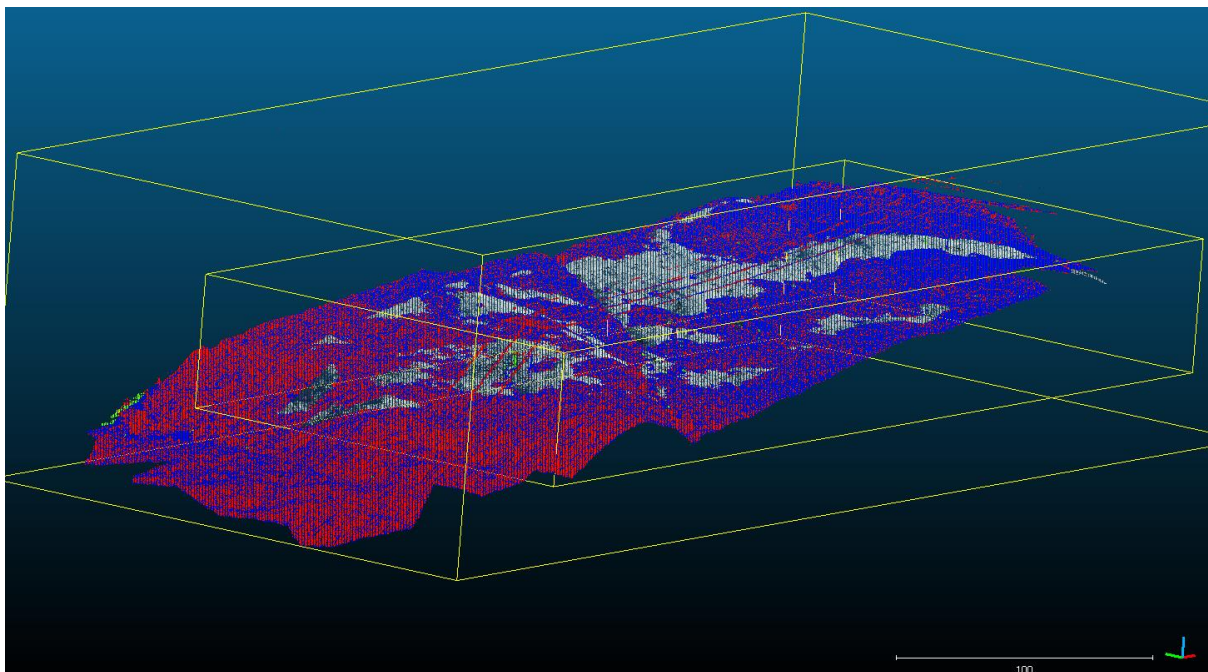


Figure 51 Cloud2Cloud distance Høydedata and MavicPRO point cloud with snow (own image)

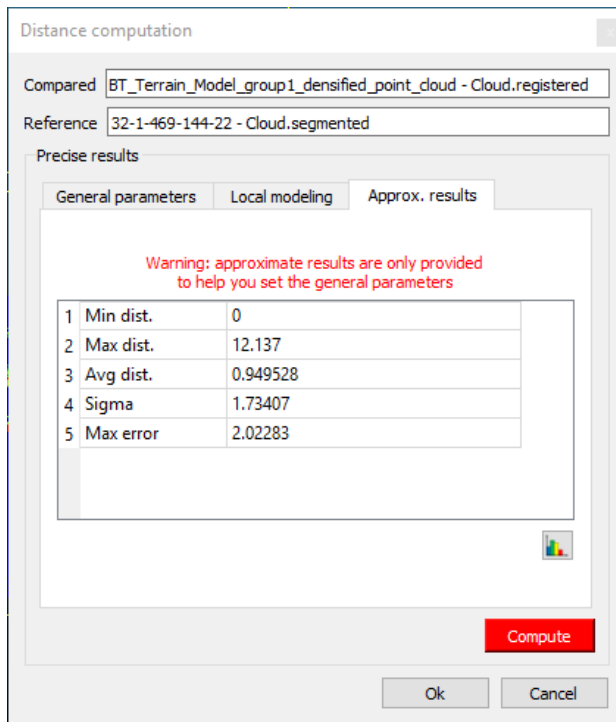


Figure 52 Distance computation between Høydedata and the MavicPRO point cloud with snow in m (own image)

Georeferencing	yes, 5 GCPs (5 3D), mean RMS error = 0.115 m
-----------------------	--

Figure 53 RMS error of GCPs (own image)

Table 7 Flight pattern differences between 2 flights (own table)

Photo	Flight 1		Flight 2		Differences		Vector
	X	Y	X'	Y'	ΔX	ΔY	Distance
1	6692929,87	303327,50	6692929,06	303327,36	0,81	0,14	0,82201
8	6692929,34	303396,29	6692930,69	303396,61	1,35	0,32	1,387408
18	6692929,29	303495,62	6692930,75	303495,83	1,46	0,21	1,475025
28	6692929,30	303595,17	6692930,66	303594,97	1,36	0,20	1,374627
38	6692929,30	303694,63	6692930,58	303694,32	1,28	0,31	1,317004
41	6692906,57	303691,87	6692907,74	303691,76	1,17	0,11	1,17516
48	6692906,71	303622,06	6692908,16	303622,20	1,45	0,14	1,456743
62	6692906,78	303483,07	6692908,20	303483,11	1,42	0,04	1,420563
72	6692906,80	303383,72	6692908,21	303383,93	1,41	0,21	1,425553
78	6692907,39	303325,66	6692906,03	303325,80	1,36	0,14	1,367187
80	6692885,96	303324,72	6692887,37	303324,90	1,41	0,18	1,421443
84	6692884,37	303362,73	6692885,71	303362,20	1,34	0,53	1,441007
101	6692884,38	303531,03	6692885,77	303530,99	1,39	0,04	1,390575
111	6692884,24	303630,24	6692885,75	303630,16	1,51	0,08	1,512118
117	6692884,22	303689,17	6692885,66	303689,35	1,44	0,18	1,451206
120	6692862,24	303678,69	6692863,53	303678,69	1,29	0,00	1,29
124	6692861,87	303639,14	6692863,34	303639,12	1,47	0,02	1,470136
145	6692862,00	303430,61	6692863,37	303430,67	1,37	0,06	1,371313
153	6692862,04	303351,24	6692863,38	303351,33	1,34	0,09	1,343019
156	6692860,77	303323,13	6692862,25	303323,28	1,48	0,15	1,487582
159	6692839,74	303330,49	6692841,15	303330,65	1,41	0,16	1,419049
172	6692839,49	303459,39	6692840,91	303459,68	1,42	0,29	1,44931
189	6692839,45	303628,56	6692840,95	303628,95	1,50	0,39	1,549871
Mean					1,37	0,17	1,383387

12.2 Discussion of the results

12.2.1 Overlap

To ensure good results, a point that is generated in the point cloud should be visible from as much pictures as possible (see Figure 40 and Figure 41). More pictures eliminate uncertainty, thus making the point cloud more accurate and more usable. All of the software recommended that each point should be visible from at least 4 pictures, and more than 5 pictures was found to be ideal.

12.2.2 Error contribution

Several factors induce errors of various magnitudes in the point cloud. The main ones are the GPS/GNSS systems, the GCP's and lack thereof, internal camera parameters, imaging settings (overlap, flying altitude, angles, etc..) and the processing of the pictures to a point cloud. (Fei Dai, 2014)

As can be seen in Figure 53, the RMS error of the GCP's in this case is approximately 11cm. This is caused due to the form and color of the GCP's. Pix4D uses an algorithm based on the colour of neighbouring pixels. The targets we used (black plastic with pink squares spray painted on them) were too small and the used colours were hard to discern. This made the process more inaccurate. The use of different, better suited GCP's could reduce this error.

12.2.3 Total inaccuracy and uncertainty

The largest difference between the drones is found in the absolute georeferencing variance. It is easily visible in Table 4, Table 5, Figure 44 and Figure 45. The absolute variance of the MavicPro drone is somewhere in the range of 3 and -3m, while most of the errors of the Phantom4RTK drone are in the range of 0.02 to -0.02m. This is accomplished by the RTK system of the drone. The RMS error of the GCP's in this case is approximately 0.11m. This means that the absolute accuracy in this case is around 0.11m.

Another part of the variance is the relative geolocation variance. This is mainly dependant on the reconstruction quality. This is influenced by the camera, the overlap of images, etc. A general rule of thumb is to take 2 to 3 times (Pix4D, 2018) the GSD to calculate this variance. In our case, as can be seen in Table 1, this is approximately 0.0535 m for both drones.

For increased accuracy of the geolocation, it is recommended to use at least 3 GCP's. We used 5 GCP's to get the best results possible. These ensure correct geolocation of the images, which increases the accuracy of the point cloud.

<https://support.pix4d.com/hc/en-us/articles/202558889-Accuracy-of-Pix4D-outputs>

12.2.4 Processing time and load

As can be read in Figure 14 and Figure 42, processing load is very similar between the programs. The most notable differences can be found in the processing time. Some renderings were done in a couple of hours, while others took up more than an entire day. Hence, we advise against using Agisoft, due to the extraordinarily processing time and limited functionality as discussed on pages 17 and 18.

ARCGIS Drone2Map had the additional issue of having LOD (Level Of Detail) errors. These were created because the amount of data that was being processed, wasn't limited according to the specs of the computer. This forced us to lower the quality of the data significantly thus increasing the error and uncertainty in the cloud. Therefore, it is recommended to use a computer with preferably more than 8GB of RAM. For projects with more than 100 images, 16 GB of RAM is recommended by the standard specifications of the software (ARCGIS, 2018).

Certain processes took a considerable amount of time in Agisoft Metashape Professional. The processing of the dense point cloud took approximately 22 hours. Other programs did similar processing tasks in a bit more than one tenth of this time. Thus, we advise against the use of this software solution.

12.3 Influence of snow on results

In case of snow, the algorithm used by the software has difficulty with accurately finding corresponding pixels between the pictures. Because of the monotone colour and flatness due to the snow, it is harder to compute matches. Pix4D advises a high frontal and side overlap to offset these problems. The frontal overlap should be 85%, and the side overlap 75%. Adjusting the settings of the camera to achieve a higher contrast is advised. Lastly, the drone should maintain a higher altitude.

As can be seen on Figure 51 and Figure 52 there was some noticeable influence of snow on the point clouds. More areas of the point cloud with snow are visible above Høydedatas point cloud. The mean distance between the point clouds is also in the metres range instead of the decimetres range. This implies that there is a certain offset, due to the snow.

12.4 Comparison with Høydedata

Figure 48 shows the calculated difference between a registered point cloud and a point cloud from Høydedata. The Pix4D point cloud has been translated with the use of one known point, measured with a total station. The coordinates of the known point and the coordinates in the Pix4D point cloud differed greatly. For the y axis, the difference was almost a metre, and the z axis had a difference of 43.30m. Only the x-axis was within reasonable distance of the known point, with an inaccuracy of approximately 0.08m. The difference between these points were calculated and the point cloud was translated according to the results of the calculations. After this procedure, the point cloud was within reasonable accuracy of the data from Høydedata.

As can be seen in Figure 47, Figure 48 and Figure 50, the distance after the registering through the known point or the GCP's is within 0.1m level. The large maximum distance and error can be attributed to the noise from the power towers we weren't able to filter out entirely.

The extreme variance in the z-axis of the point cloud can be attested to the height system used by Pix4D and the drone (Pix4D, 2019). The drone uses an ellipsoidal system, while Pix4D uses an orthometric system. It is recommended to change the system before importing the pictures into Pix4D. In the area of measurement the difference between the systems was approximately 43.30m.

12.5 Flight plan accuracy

One of the great advantages of using drones is that the programmed flight patterns can be repeated over and over, with very reasonable accuracy. Table 7 indicates that the distance between the geolocation of pictures taken is within 1.4m. The point clouds generated are almost identical after translation as can be seen in Figure 48 and Figure 50.

12.6 Comparison with terrestrial laserscanning

Even though terrestrial laserscanning and aerial photogrammetry yield comparable results, the process of acquiring and processing data are completely different. Both have clear strengths and weaknesses compared to each other. Some are more apparent than others.

Practical experiences

One of the main differences between the terrestrial scanning and the aerial photogrammetry is in the datasets. They both provide the method and ease of use. The usage of the laserscanner takes significantly more time and equipment than the drone. This makes the drone more useful for remote and hard to access places, since the equipment needed is far less and lighter than the laserscanner's.

For the datasets, the main difference is the applications for which the data is viable. Due to limitations with the drone, it was clear it isn't suited nearly as well for imaging the tower as the laserscanner. This was due to the angle the pictures were taken through a preplanned flight pattern. Even with pictures from around the tower taken in freeflight, the model was still far less usable compared to the model of the terrestrial laserscanner. This was due to the limited amount of overlap on the pictures taken, and how narrow the steel beams on the electricity pylon are. On the other hand, the drone is easier and much faster to use to acquire the data for a terrain model. Generally, the drone is thus more suited for the applications of this report.

Table 8 Equipment for surveys (own table)

Drone Photogrammetry	Laser scanner
1 drone scanner	1 laser scanner
1 RTK station	5 tripods
5 gcp's	1 totalstation
1 GNSS system	3 targets
	1 GNSS system
	1 prisma
	1 jual pole tripod
	1 jual pole

Comparison devices

Our main point of interest was the technical limitations and strengths of both techniques. After registering the data without snow, the laserscanner achieved an accuracy of 0.004m. The error produced is highly dependant on the settings of the drone, and the used software. Initially, the accuracy of the laserscanner was far superior to the accuracy of both drones.

Due to mistakes made while georeferencing the final error was around 0,018m as can be seen in Table 2. The reason of this larger error is the way of georeferencing the laserscanning group used. This induced a larger than average error into the geolocation process. The relative error of the drone is approximately 0.063 m as shown in Table 3 Relative uncertainties calculated from concrete foundationTable 3. This error stems from the generation of the point cloud. The theoretical value for this error was 0.048m. The difference between the theoretical and calculated error stems from the fact that relative accuracy can differ in different areas of the point cloud. The geolocation errors are similar to the laserscanning, since we used the same technique for this. The RMS error of our GCP's is 0.111m. This means that the laserscanner is still way more accurate than the drones.

12.7 Conclusion of the report

The use of drones as replacement for the current aerial LiDAR scanning is dependant on a few factors. In some cases the drones are the best solution, in others the aerial LiDAR. For some select applications, a laserscanner is the most suitable option.

The main factors for use of a drone are batteries, visibility and accessibility of an area. Batteries limit the time a drone can be used for data acquisition. This problem can be circumvented by using a system with spare batteries. The distance a drone can be used at is still limited, because of the fact that the pilot should always keep the drone in his/her line of sight. Therefore, the technique can't be used for very long distance jobs, unless a segmented approach is used. Lastly, if an area is too remote or too hard to access, a drone is not a feasible option. Visibility of the drone becomes can become an issue in this case, since you have to be in proximity of the photographed area to keep an eye on the drone.

Aerial LiDAR is still the best option for long distance jobs and data acquisition in remote or hard to access areas. The only reason for this is the current limitations of the drones and the fact that you have to keep the drone in sight during the flight.

Finally, for detailed models of the towers, a laserscanner is the best option. Data provided by this solution has the highest point density, and the best accuracy of the techniques. The point density for the towers was a problem with photogrammetry, due to the size of the steel beams of the tower, the flying height and the angles of the pictures taken. One limiting factor is the accessibility of the tower area and the weight and amount of equipment. Due to these factors, aerial LiDAR is still the best option for some cases.

13 References

- Agisoft. (2019). *Features*. Retrieved from Agisoft:
<https://www.agisoft.com/features/professional-edition/>
- ARCGIS. (2018). *System requirements*. Retrieved from ARCGIS Drone2Map help:
<https://doc.arcgis.com/en/drone2map/get-started/system-requirements.htm>
- Charles D. Ghilani, P. R. (2012). Elementary surveying, an introduction to geomatics. In P. R. Charles D. Ghilani, *Elementary surveying, an introduction to geomatics* (pp. Chapter27, P.819-862). Paerson .
- Corke , P. (Director). (2012). *Image geometry and planar homography* [Motion Picture].
- Dennis Morgan, E. F. (2001). *erial Mapping: Methods and Applications, Second Edition*. In E. F. Dennis Morgan, *erial Mapping: Methods and Applications, Second Edition* (pp. chapter6 p.29-39). Lewis publishers .
- DJI. (2019). *d-rtk-2 high precision GNSS mobile station*. Retrieved from DJI:
<https://www.dji.com/no/d-rtk-2>
- DJI. (2019). *Mavic Pro*. Retrieved from dji: https://www.dji.com/no/mavic-2-enterprise?site=brandsite&from=insite_search
- DJI. (2019). *phantom 4 rtk*. Retrieved from dji: https://www.dji.com/no/phantom-4-rtk?site=brandsite&from=insite_search
- Fei Dai, Y. F. (2014). *Photogrammetric error sources and impacts on modeling and surveying in construction engineering applications*. Retrieved from viejournal:
<https://viejournal.springeropen.com/articles/10.1186/2213-7459-2-2>
- Hodler, X. Y. (14 Mar 2013.). Visual and Statistical Comparisons of Surface Modeling Techniques for Point-based Environmental Data. 165-175.
- Hodler, X. Y. (14 Mar 2013). Visual and Statistical Comparisons of Surface Modeling Techniques for Point-based Environmental Data. 165-175.
- Høydedata. (2016). *LaserInnsyn*. Retrieved from Høydedata:
<https://hoydedata.no/LaserInnsyn/>
- J. Valente, D. S. (2013). Near-optimal coverage trajectories for image mosaicing using a mini quad-rotor over irregular-shaped fields,” in Precision agriculture,. In D. S. J. Valente, *Near-optimal coverage trajectories for image mosaicing using a mini quad-rotor over irregular-shaped fields,” in Precision agriculture,* (pp. Vol 14(1), pp. 115-132,).
- L. H. Nama, L. H. (2016). *An Approach for Coverage Path Planning for UAVs*. School of Engineering. Computer and Mathematical Sciences Auckland University of Technology, Auckland, New Zealand,State Key Laboratory of Digital Manufacturing Equipment and Technology Huazhong University of Science and Technology, Wuhan, China: School of Engineering. Computer and Mathematical Sciences Auckland University of Technology, Auckland, New Zealand,State Key Laboratory of Digital Manufacturing Equipment and Technology Huazhong University of Science and Technology, Wuhan, China.
- L. H. Nama, L. H. (n.d.). *An Approach for Coverage Path Planning for UAVs*. School of Engineering. Computer and Mathematical Sciences Auckland University of Technology, Auckland, New Zealand,State Key Laboratory of Digital Manufacturing Equipment and Technology Huazhong University of Science and Technology, Wuhan, China: School of Engineering. Computer and Mathematical Sciences Auckland University of Technology, Auckland, New Zealand,State Key Laboratory of Digital Manufacturing Equipment and Technology Huazhong University of Science and Technology, Wuhan, China.

- Norwegian Ministry of Petroleum and Energy. (2015). *THE ELECTRICITY GRID*. Retrieved from Energifaktanorge: <https://energifaktanorge.no/en/norsk-energiforsyning/kraftnett/>
- Pix4D. (2018, August). *Accuracy of Pix4D outputs*. Retrieved from Pix4D Support.
- Pix4D. (2019). *A project from A to Z*. Retrieved from Pix4D Support: <https://support.pix4d.com/hc/en-us/articles/202557459-Step-1-Before-Starting-a-Project-1-Designing-the-Image-Acquisition-Plan-a-Selecting-the-Image-Acquisition-Plan-Type#label5>
- Pix4D. (2019). *Orthometric vs ellipsoidal height*. Retrieved from Pix4D Support: <https://support.pix4d.com/hc/en-us/articles/202559869-Orthometric-vs-ellipsoidal-height>
- Rieke, M., Foerster, T., Geipel, J., & Prinz, T. (2011). HIGH-PRECISION POSITIONING AND REAL-TIME DATA PROCESSING OF UAVSYSTEMS. In *International Archives of the Photogrammetry, Remote Sensing and Spatial Information Sciences, Volume XXXVIII-1/C22* (pp. 119-124). Zurich, Switzerland.
- Thomas M. Lillesand, R. W. (2004). Remote sensing and image interpretation, fifth edition. In R. W. Thomas M. Lillesand, *Remote sensing and image interpretation, fifth edition*. Wiley.
- Van Sickle, J. (2008). *GPS for land surveyors*. U.S.: CRC Press.
- Y. Li, H. C. (2011). Coverage path planning for UAVs based on enhanced exact cellular decomposition method,. In H. C. Y. Li, *Coverage path planning for UAVs based on enhanced exact cellular decomposition method*, (pp. Vol. 21(5), pp. 876-885).
- Y. Li, H. C. (2011.). Coverage path planning for UAVs based on enhanced exact cellular decomposition method,. In H. C. Y. Li, *Coverage path planning for UAVs based on enhanced exact cellular decomposition method*, (pp. Vol. 21(5), pp. 876-885).

14 List of figures

Figure 1 Types of towers (Norwegian Ministry of Petroleum and Energy, 2015)	6
Figure 2 Energy production and consumption in Norway (Norwegian Ministry of Petroleum and Energy, 2015)	6
Figure 3 Electricity pylon at test site (own image).....	7
Figure 4 Test area (Høydedata, 2016).....	8
Figure 5 Dji Mavic Pro (DJI, 2019)	10
Figure 6 Dji Phantom 4 RTK (DJI, 2019)	10
Figure 7 Dji D-RTK 2 base station (own image).....	11
Figure 8 Mavic during system test (own image).....	12
Figure 9 Mavic on base station (own image).....	12
Figure 10 GCP target (own image).....	13
Figure 11 Coordinates GCP (own image)	13
Figure 12 GCP from drone image (own image).....	13
Figure 13 Software solutions (own image)	14
Figure 14 Computer specifications (own image)	14
Figure 15 Pix4D point cloud (own image).....	15
Figure 16 Pix4D options	15
Figure 17 Flight pattern (own image)	15
Figure 18 Pix4D user interface (own image).....	17
Figure 19 Agisoft Metashape Professional point cloud (own image).....	17
Figure 20 Agisoft Metashape Professional user interface (own image).....	18
Figure 21 ARCGis Drone2Map point cloud (own image)	19
Figure 22 ARCGis Drone2Map user interface (own image).....	20
Figure 23 RTK antenna on UAV (DJI, 2019).....	21
Figure 24: types of aerial photogrammetry (L. H. Nama, An Approach for Coverage Path Planning for UAVs, 2016).....	23
Figure 25 (L. H. Nama, An Approach for Coverage Path Planning for UAVs, 2016).....	24
Figure 26 (Thomas M. Lillesand, 2004).	24
Figure 27 (Corke , 2012).....	25
Figure 28 (Corke , 2012).....	26
Figure 29 (Corke , 2012).....	27
Figure 30 (Corke , 2012).....	27
Figure 31 (Corke , 2012).....	28
Figure 32 (Corke , 2012).....	28
Figure 33 End-lap on two consecutive photos in a flight line (L. H. Nama, An Approach for Coverage Path Planning for UAVs, 2016).....	29
Figure 34 Side-lap between two adjacent flight lines (L. H. Nama, An Approach for Coverage Path Planning for UAVs, 2016).	31
Figure 35 Side-lap on three adjacent flight lines (L. H. Nama, An Approach for Coverage Path Planning for UAVs, 2016).....	31
Figure 36 clean area of a stereomodel (L. H. Nama, An Approach for Coverage Path Planning for UAVs, 2016).....	32
Figure 37 a) Von Neumann neighbourhood b) Moore neighbourhood (L. H. Nama, An Approach for Coverage Path Planning for UAVs, 2016).....	34
Figure 38 (L. H. Nama, An Approach for Coverage Path Planning for UAVs, 2016).....	35
Figure 39: a single point projected out of 4 images (own image)	36

Figure 40 Image overlapping from MavicPro drone (own image).....	37
Figure 41 Image overlapping from Phantom4RTK drone (own image)	38
Figure 42 Processing time and load per software solution (own image)	38
Figure 43 Known points on concrete foundation	39
Figure 44 Graph of the absolute geolocation variance of the Phantom4RTK drone (own table)	41
Figure 45 Graph of the absolute geolocation variance of the MavicPRO drone (own table).....	41
Figure 46 Distance computation between Høydedata and original Phantom4RTK point cloud in m (own image)	42
Figure 47 Cloud2Cloud distance Høydedata and original point cloud (own image)	42
Figure 48 Distance computation between Høydedata and translated Phantom4RTK point cloud in m (own image)	43
Figure 49 Cloud2Cloud distance Høydedata and translated point cloud (own image)	43
Figure 50 Distance computation between Høydedata and the GCP registered Phantom4RTK point cloud in m (own image)	44
Figure 51 Cloud2Cloud distance Høydedata and MavicPRO point cloud with snow (own image)	44
Figure 52 Distance computation between Høydedata and the MavicPRO point cloud with snow in m (own image)	45
Figure 53 RMS error of GCPs (own image)	45

15 List of tables

Table 1 Influence of GSD on general accuracy after processing (own table)	37
Table 2 Errors of measured points from the laserscanning data (own table)	38
Table 3 Relative uncertainties calculated from concrete foundation (own table).....	39
Table 4 Absolute geolocation variance Phantom4RTK (own table)	40
Table 5 Absolute geolocation variance MavicPRO (own table)	40
Table 6 Calculation of translation (own table).....	42
Table 7 Flight pattern differences between 2 flights (own table)	45
Table 8 Equipment for surveys (own table).....	48